

See discussions, stats, and author profiles for this publication at: <https://www.researchgate.net/publication/23807911>

Periplasmic Loop P2 of the MalF Subunit of the Maltose ATP Binding Cassette Transporter Is Sufficient To Bind the Maltose Binding Protein MalE

ARTICLE *in* BIOCHEMISTRY · MARCH 2009

Impact Factor: 3.02 · DOI: 10.1021/bi801376m · Source: PubMed

CITATIONS

18

READS

32

7 AUTHORS, INCLUDING:



Tomas Jacso

Nuevolution A/S

8 PUBLICATIONS 104 CITATIONS

[SEE PROFILE](#)



Martin Daus

Robert Koch Institut

26 PUBLICATIONS 207 CITATIONS

[SEE PROFILE](#)



Peter Schmieder

Leibniz-Institut für Molekulare Pharmakol...

119 PUBLICATIONS 3,180 CITATIONS

[SEE PROFILE](#)



Bernd Reif

Technische Universität München

124 PUBLICATIONS 4,263 CITATIONS

[SEE PROFILE](#)

Periplasmic Loop P2 of the MalF Subunit of the Maltose ATP Binding Cassette Transporter Is Sufficient To Bind the Maltose Binding Protein MalE[†]

Tomas Jacso,[‡] Mathias Grote,[§] Martin L. Daus,[§] Peter Schmieder,[‡] Sandro Keller,[‡] Erwin Schneider,[§] and Bernd Reif*,^{‡,||}

Leibniz-Institut für Molekulare Pharmakologie (FMP), Robert-Rössle-Strasse 10, D-13125 Berlin, Germany, Institut für Biologie, AG Bakterienphysiologie, Humboldt-Universität zu Berlin, Chausseestrasse 117, D-10115 Berlin, Germany, and Charité Universitätsmedizin, D-10115 Berlin, Germany

Received July 23, 2008; Revised Manuscript Received January 16, 2009

ABSTRACT: The *Escherichia coli* maltose transporter belongs to the ATP binding cassette (ABC) transporter superfamily. Recently, the crystal structure of the full transporter MalFGK₂ in complex with the maltose binding protein (MBP) was determined [Oldham, M. L., et al. (2007) Crystal structure of a catalytic intermediate of the maltose transporter. *Nature* 450, 515–522]. Using liquid-state NMR, we find that the periplasmic loop P2 of MalF (MalF-P2) folds independently in solution and adopts a well-defined tertiary structure which is similar to the one found in the crystal. MalF-P2 interacts with the maltose binding protein, independent of the transmembrane region of MalF and MalG with an affinity of ~10–20 μM, in the presence and absence of substrate. Analysis of residual dipolar coupling (RDC) experiments shows that the conformation of the two individual domains of MalF-P2 is preserved in the absence of MalE and resembles the conformation in the X-ray structure. Upon titration of MalE to MalF-P2, the two domains of MalF-P2 change their relative orientation to accommodate the ligand. In particular, a conformational change of domain 2 of MalF-P2 is induced, which is distinct from the conformation found in the X-ray structure.

ATP binding cassette (ABC)¹ transporters are ubiquitous membrane protein complexes that use the energy generated from ATP hydrolysis to transport solutes across the membrane (*1*). In bacteria, the majority of ABC transporters are importers that consist of a substrate-binding protein, two integral membrane components, and two membrane-associated ATP binding cassettes. One classical representative is the maltose transporter of *Escherichia coli/Salmonella* composed of the periplasmic maltose binding protein (MBP) MalE, the two integral cytoplasmic membrane proteins MalF and MalG, and two copies of the ATPase subunit MalK (*2*). In bacteria and archaea, binding proteins are the main determinants of substrate specificity. The determination of the crystal structure of the reconstituted maltose transport MalFGK₂ in complex with MalE has recently drawn a lot of attention to this system (*3*). There, the large periplasmic loop P2 of MalF (MalF-P2) is in contact with MalE from which maltose has already been released. In fact, MalF-P2 seems to act as a receptor which recruits MalE, and thus maltose, to the pore of the membrane protein. We are attempting to understand if this interaction occurs as well in

solution. An alternative docking site might involve the periplasmic loop P3 of MalG which interacts with the maltose binding site of MalE in the X-ray structure. The question of how much MalF-P2 contributes to substrate recognition is still unresolved. Earlier genetic and biochemical investigations show that both MalF and MalG are involved in binding to the substrate-binding protein MalE (*4, 5*). It could be demonstrated that the N-terminal lobe of MalE interacts with MalG, whereas the C-terminal part of MalE is close in space to MalF. We find that MalF-P2 interacts with MalE in a manner independent of maltose. We show that MalF-P2 adopts a well-defined tertiary structure independent of other parts of the transporter.

MATERIALS AND METHODS

Plasmid Design. A DNA fragment of the MalF gene of *E. coli* encompassing codons 93–275 was amplified by polymerase chain reaction (PCR). According to the topology of MalF, this fragment covers the entire P2 loop sequence (*3, 6*). The fragment was subcloned into expression vector pET-15 (Novagen), resulting in plasmid pMG15. The plasmid integrity was verified by nucleotide sequencing. Cysteine residues replacing MalF-P2(T177), MalE(T31), and MalE-K179 were introduced by Stratagene's Quikchange kit using plasmids pMG15 and pCB6 (*5*) as templates for *malFP2* and *malE*, respectively. The resulting plasmids were named pMM57 (MalF-T177C), pMM47 (MalE-K179C), and pMM55 (MalE-T31C).

Expression and Purification. (*i*) **MalF-P2.** Uniformly ¹⁵N-labeled MalF-P2, ¹⁵N- and ¹³C-labeled MalF-P2, and ¹⁵N-,

* This work was supported by the Leibniz-Gemeinschaft and the DFG (Grants RE1435, SCHN274, SFB 449, and SFB 740).

† To whom correspondence should be addressed. E-mail: reif@fmp-berlin.de. Phone: +49 30 94791-191. Fax: +49 30 94793-199.

‡ Leibniz-Institut für Molekulare Pharmakologie (FMP).

§ Humboldt-Universität zu Berlin.

|| Charité Universitätsmedizin.

¹ Abbreviations: NMR, nuclear magnetic resonance; RDCs, residual dipolar couplings; ABC, ATP binding cassette; MBP, maltose binding protein; TMD, transmembrane domain.

¹³C-, and ²D-labeled MalF-P2 were overproduced in *E. coli* BL21 DE3 (pLysS) harboring plasmid pMG15. ¹⁵N-labeled protein was amplified using ¹⁵NH₄Cl as the sole nitrogen source. ¹³C labeling and ²H and ¹³C labeling were achieved using [¹H, ¹³C]glucose and [²H, ¹³C]glucose, respectively, as the carbon source. Deuterated protein was prepared using 99.9% D₂O in M9 minimal medium. The cell lysate was incubated for 4 h at 4 °C with an equilibrated nickel matrix (Ni Sepharose 6 Fast Flow, GE Healthcare). The column was washed with 25 mM imidazole to prevent unspecific binding. The protein was eluted at an imidazole concentration of 250 mM. The N-terminal His tag was cleaved off by thrombin digestion (Thrombin CleanCleave kit, Sigma, Deisenhofen, Germany). The protein solution was dialyzed and, as a final purification step, subjected to a Superdex 75 gel filtration column to remove residual imidazole, His tag fragments, and any impurities. MalF-P2 is monomeric in solution under the conditions employed in this study as shown by analytical ultracentrifugation (Supporting Information).

(ii) *MalE (MBP)*. Polyhistidine-tagged MalE was overproduced in strain JM109 harboring plasmid pCB6 and purified as described in ref 5.

Cross-Linking. Cross-linking experiments were performed as described previously (7) using Cu(1,10-phenanthroline)SO₄ (CuPhe) to covalently link two proteins.

Sample Preparation. (i) *NMR Spectroscopy*. MalF-P2 samples were measured in 20 mM phosphate buffer (pH 7.4) with and without 500 μM maltose, 100 mM NaCl, 0.01% NaN₃, and 10% D₂O as the lock solvent, at protein concentrations ranging from 0.5 to 1.0 mM. Dipolar coupling measurements were carried out using liquid-crystalline Pf1 filamentous phages (purchased from Profos AG) as an alignment medium at a concentration of 7 mg/mL (residual quadrupolar coupling of ²H₂O splitting ~ 17.5 Hz), as described by Yang et al. (8). Titration experiments were performed using [MalF-P2]:[MalE] molar ratios of 10:1, 1:1, and 1:8, in the presence and absence of 1 mM maltose.

(ii) *ITC*. To prepare protein samples for ITC titration experiments, 2 mL of 1 mM solutions of MalE and MalF-P2 was dialyzed (Spectral/Por, Spectrum Laboratories Inc.) individually in 20 mM phosphate buffer [100 mM NaCl (pH 7.4)] with and without maltose (employing concentrations ranging from 500 μM to 100 mM), overnight at 7 °C with light stirring. MalE (700–800 μM) and MalF-P2 (50 μM) were filtered, degassed, and inserted into the injection syringe and calorimeter cell.

NMR Experiments and Analysis. NMR data were recorded by using Bruker 600 and 750 MHz spectrometers (Bruker Biospin, Karlsruhe, Germany), both equipped with triple-resonance cryogenic probes. For backbone and side chain assignments of MalF-P2, standard triple-resonance experiments (¹⁵N HSQC-TROSY, HNCA, CBCANH, CBCA-CONH, ¹³C TOCSY-HMQC, ¹³C COSY-HMQC, HCCH-TOCSY, and HCCH-COSY) (9) were conducted, adjusting the sample temperature to 27 °C. ¹⁵N T₁ and T₂ relaxation rates were determined as described in ref 10, and the calculated overall correlation times (τ_c) were compared to tabulated values of τ_c for globular proteins of different sizes to estimate the dynamical character of MalF-P2 (11, 12). ¹⁵N HSQC IPAP (13) and J-resolved HNCO, HNCA pulse experiments (14) were employed to determine the residual

dipolar couplings (RDCs) (N_iH_i^N, Cα_iC'_i, Hα_iCα_i) of MalF-P2 in its free form. After addition of MalE, ¹H-¹⁵N HSQC and ¹H-¹⁵N HSQC-TROSY experiments were used to measure N_iH_i^N RDCs. All NMR data were processed using XWIN-NMR and Topspin (Bruker Biospin) and analyzed with CCPN (15). Backbone dihedral angle prediction was performed using ¹⁵N, ¹³C', ¹³Cα, and ¹³Cβ chemical shifts of MalF-P2 after correction for ²H isotopic effects (16). Structural restraints were generated using TALOS (17). The experimental residual dipolar couplings (RDCs) were correlated against amino acids N93–K275 of the crystal structure of the *E. coli* maltose transporter (Protein Data Bank entry 2R6G) (3), employing the molecular alignment prediction program PALES (18). Dipolar couplings were fitted using the best-fit module of the program. Three data sets of dipolar couplings (two data sets for free MalF-P2 and one data set in complex with MalE) were correlated to amino acids N93–K275 (full-length MalF-P2), N93–G260 (full-length MalF-P2 without the C-terminus), N93–S113 and P209–T259 (MalF-P2, domain 1), and G117–T207 (MalF-P2, domain 2) of MalF-P2 of the X-ray structure.

ITC Experiments and Analysis. High-sensitivity microcalorimetry (19) was performed on a VP-ITC instrument (MicroCal Software, Northampton, MA). Experiments were performed at 5 and 25 °C with MalE protein solutions in the calorimeter cell and MalF-P2 solutions in the injection syringe. The time spacings between the injections were sufficiently long to allow for complete re-equilibration (600 s). Typically, 20–40 injections were performed. Baseline subtraction and peak integration were accomplished using Origin 5.0 as described by the manufacturer (MicroCal Software). Curve fitting was performed with a nonlinear fit based on a one-site binding model. The first injection was always excluded from evaluation because it usually suffers from sample losses due to mounting of the syringe and equilibration preceding the actual titration.

Crystal Structure Analysis. Structure interpretations of the crystal structure of the maltose transporter (3) were done with CCP4i 1.3.20 (Computational Project, Number 4, 1994) (20) and PyMol (21). Secondary structure elements of MalF-P2 in the X-ray structure were extracted using the dss algorithm in PyMol. Atom–atom distance searches, between MalE and MalF-P2 in the crystal structure of the maltose transporter, were set within the range of 0.0–5.0 Å; 417 contacts shorter than 5.0 Å between MalF-P2 and MalE are found for 35 residues in the N-terminal lobe of MalE and 24 residues in MalF-P2 (Figure 6). All distances originate from heavy atoms N, C, and O.

RESULTS

Figure 1A displays a structural representation of MalF-P2 in the context of the full maltose transporter. MalF-P2 is colored red. Protein Data Bank entry 2R6G (3) was employed to generate the figure. To study the interactions between periplasmic loop P2 of MalF and the maltose binding protein MalE, we expressed MalF-P2 (amino acids N93–K275) (6) as an individual protein. We find that MalF-P2 folds independently. The ¹H-¹⁵N HSQC correlation yields a well-resolved spectrum indicating that the P2 loop of MalF is well-structured (Figure 1B). Analytical ultracentrifugation shows that MalF-P2 is monomeric under the conditions employed in this study (see the Supporting Information).

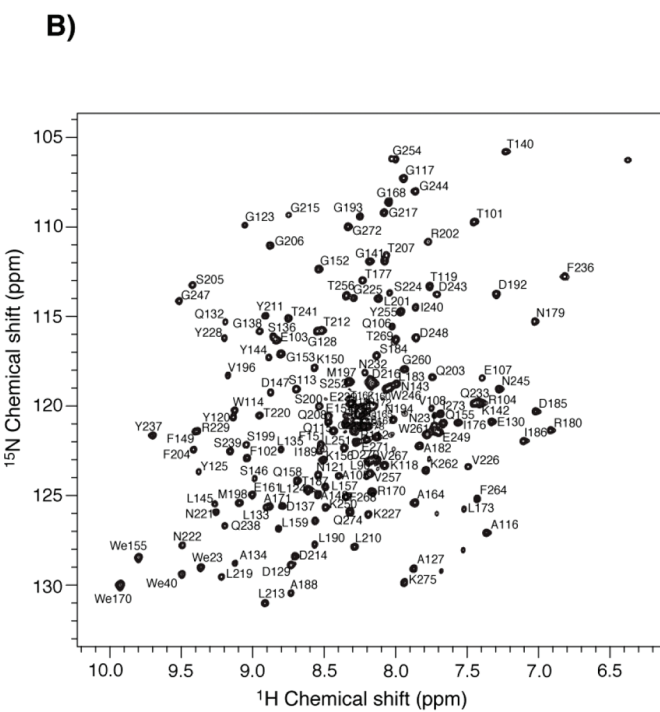
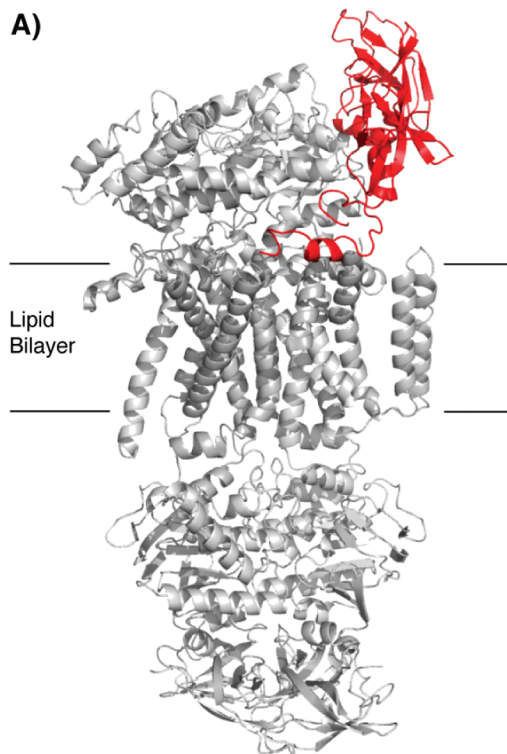


FIGURE 1: (A) MalFGK₂–MalE structure (Protein Data Bank entry 2R6G) system (3). The second periplasmic loop of MalF (MalF-P2) is colored red. (B) ^1H – ^{15}N HSQC TROSY correlation experiment with MalF-P2. The assignments of MalF-P2 are deposited in the BMRB database, as accession code BMRB-15911 (22).

^{15}N T_1 and T_2 relaxation times were determined experimentally. Analysis of the relaxation rates yields an overall correlation time of the molecule (τ_c) of 8.4 ns. This correlation time is consistent with a 15 kDa protein in solution (11, 12).

Structural Analysis of MalF-P2 in the Crystal (X-ray) and in Solution (NMR). An analysis of the $\text{Ca}/\text{C}\beta$ NMR chemical shifts allows us to directly assess the secondary structure elements that are adopted by MalF-P2 in solution. The assignment of NMR chemical shifts is based on CBCANH, CBCACONH, and HNCA correlation experiments performed with a ^2H , ^{13}C , ^{15}N isotopically enriched protein (22). After correction for ^2H secondary shifts (16), we can predict the preferentially assumed secondary structure elements using TALOS (17). Figure 2 represents a comparison of the secondary structure elements found in the X-ray structure and by NMR. The predicted secondary structure matches the crystal structure very well with the exception of the amphipathic α -helix at the C-terminus of MalF-P2. We find small differences between the X-ray and NMR secondary structure prediction. TALOS requires a minimum of three consecutive amino acids displaying the same secondary structure propensities for assignment of a secondary structure element. Therefore, β -strands $\beta 1$ and $\beta 8$, which have a length of two residues only in the X-ray structure, are missing. In addition, strands $\beta 5$ (residues 155–158) and $\beta 11$ (residues 225–230) are absent in the NMR analysis as a complete set of $\text{Ca}/\text{C}\beta$ chemical shifts for residues 154 and 229, respectively. In the X-ray structure, the side chains of aromatic residues W260, F263, and F267 are oriented in the direction of the lipid bilayer, supporting the idea that the α -helix (residues 260–269) serves as an anchor to attach MalF-P2 to the lipid bilayer. We find that the C-terminus of MalF-P2 has a decreased number of secondary structure elements in solution

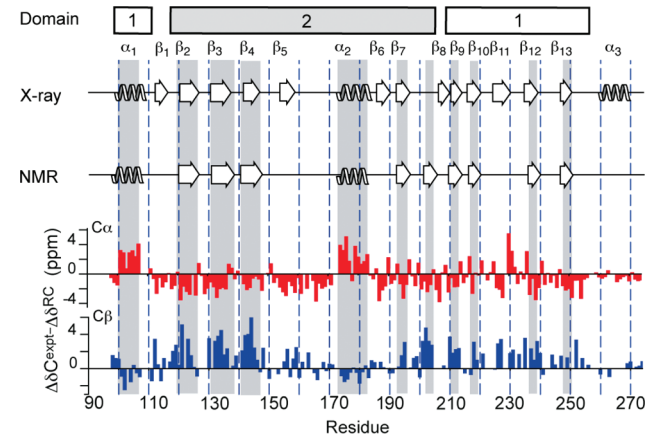


FIGURE 2: Comparison of adopted secondary structure elements of MalF-P2 in the MalFGK₂–MalE X-ray structure (3) and in the separately expressed MalF-P2 loop as predicted by NMR chemical shift analysis. The indicated secondary structure is based on the $\text{Ca}/\text{C}\beta$ NMR chemical shift data employing TALOS (17). The bottom of the figure represents differences between random coil (RC) and experimental (expt) chemical shifts for $\text{C}\alpha$ and $\text{C}\beta$ as a function of the primary sequence in MalF-P2. Secondary structure elements as predicted by TALOS are highlighted in gray. MalF-P2 folds into two individual domains (domain 1, residues 91–113 and 209–259; domain 2, residues 117–207) which are connected via β -strands $\beta 1$ and $\beta 8$.

compared to the X-ray structure. It is likely that interactions with MalF and MalG are required to induce formation of those secondary structure elements.

To probe structural differences of MalF-P2 in solution and in the crystalline state, we performed residual dipolar coupling (RDC) measurements (23, 24). Upon alignment, the anisotropic dipolar coupling is not averaged any longer. The residual dipolar component in the doublet splitting reflects directly the orientation of a particular bond vector

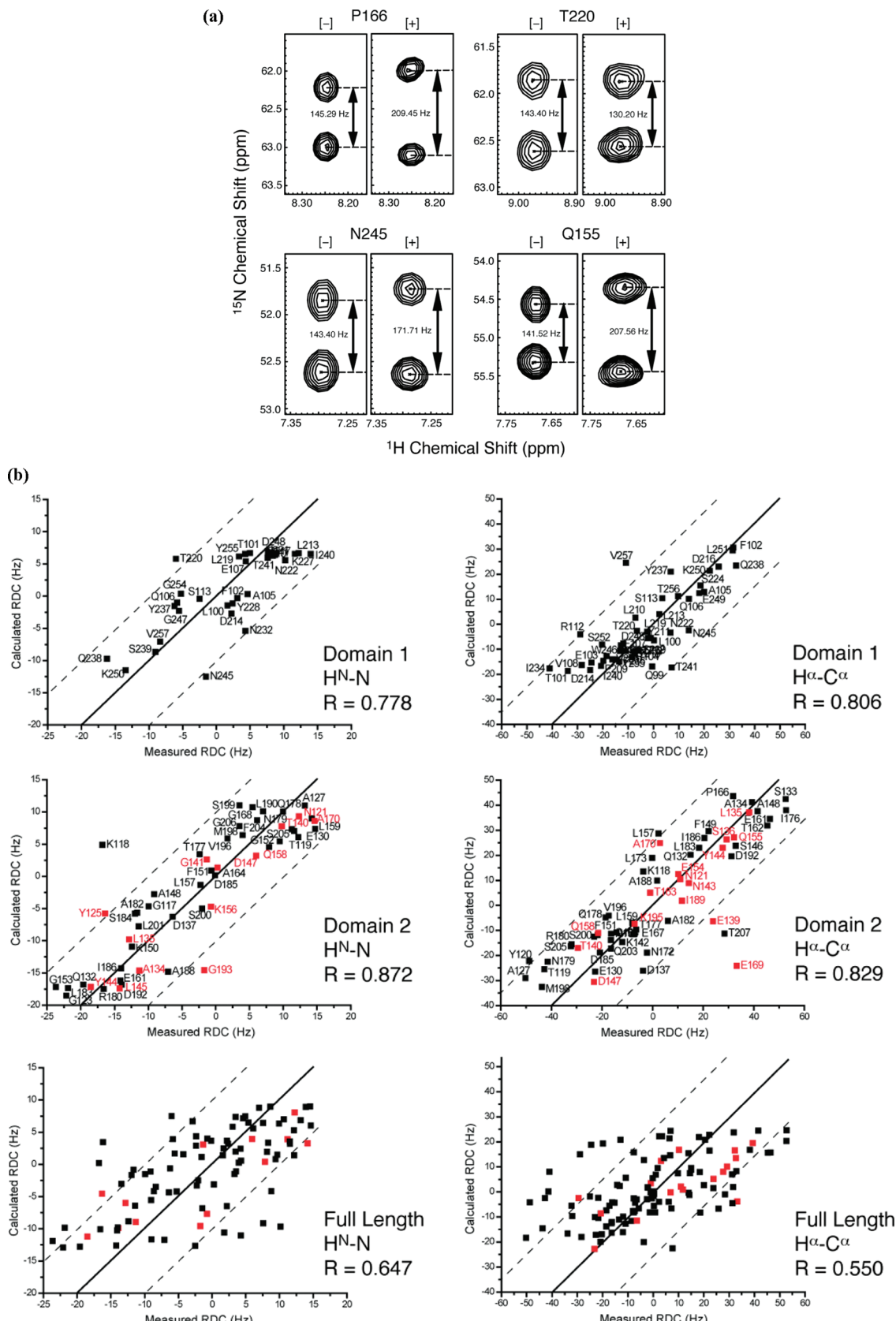


FIGURE 3: (a) $\text{H}^\alpha\text{-C}^\alpha$ residual dipolar couplings (RDCs) for selected residues in MalF-P2. Pf1 phages (7 mg/mL yielding a residual quadrupolar coupling of the D_2O resonance on the order of 17.5 Hz) were used as an alignment medium (25, 26). [-] and [+] indicate that the respective spectrum was recorded in the absence and presence of alignment medium, respectively. All spectra were recorded without maltose in the sample buffer. (b) Predicted RDC values vs experimental RDCs of MalF-P2 using PALES (18). Using $\text{H}^\text{N}\text{-N}$ and $\text{C}^\alpha\text{-H}^\alpha$ RDC data, domain 1 (residues 91–113 and 209–259) correlates with an average R value of 0.79 and domain 2 (residues 117–207) with an R value of 0.85. All experimental RDC values could be fit to the full structure of the MalF-P2 loop, yielding an average R value of 0.59. Residues which are colored red are involved in crystal contacts with a MalK molecule in the symmetry-related unit cell (see the Supporting Information).

Table 1: Correlation Coefficients Calculated by Fitting Experimental RDC Values to the X-ray Structure of the MalFGK₂•E Complex Using PALES (18)^a

		domain 1, domain 2 and domain 2 C-terminus			
		domain 1	domain 2	domain 1 and domain 2	domain 2, and C-terminus
Free MalF-P2					
H ^N –H	all amino acids excluding crystal contacts	0.78 —	0.87 0.87	0.68 0.66	0.65 0.62
H _α –C _α	all amino acids excluding crystal contacts	0.81 —	0.83 0.88	0.58 0.56	0.55 0.56
MalF-P2 and MalE					
H ^N –H	all amino acids excluding crystal contacts	0.90 —	0.52 0.58	0.64 0.70	0.64 0.69

^a High correlation coefficients indicate that the conformations in the crystal and in solution are comparable. Domain 1 consists of residues 91–113 and 209–259. Domain 2 consists of residues 117–207. Full-length MalF-P2 consists of residues 93–275. Full-length MalF-P2 without the C-terminus consists of residues 93–260.

with respect to an alignment tensor that is determined by the shape of the molecule. Knowing the structure of the protein allows a back-calculation of RDCs and yields a set of theoretically predicted residual dipolar couplings (18). Figure 3a represents spectra for four residues extracted from a *J*-resolved three-dimensional HNCA experiment that was recorded without scalar decoupling in the ¹³C evolution period. H^N–N and H_α–C_α residual dipolar couplings were fitted subsequently against the X-ray structure of MalF-P2. A correlation of those back-calculated RDCs and the experimental RDCs is shown in Figure 3b. A fairly good fit is obtained for the two individual domains alone. For domain 1, we determine a correlation coefficients (*R*) of 0.78 and 0.81 for H^N–N and H_α–C_α couplings, respectively. Similarly, we obtain a correlation coefficients (*R*) of 0.83 and 0.87 for H^N–N and H_α–C_α couplings, respectively, for domain 2. A better fit of the correlation of the individual domains and the complete P2 loop of MalF might be achievable for a higher-resolution X-ray structure. The X-ray structure of the maltose transporter (3) has a resolution of ~3 Å (root-mean-square deviation) which leaves some uncertainties concerning local structural fluctuations. No correlation is observed if all residues of the P2 loop of MalF are subjected to the fitting procedure (correlation coefficient *R* = 0.65 and 0.55 for H^N–N and H_α–C_α couplings, respectively). The fit improves only marginally when the C-terminus (residues 260–275) containing the amphipathic helix is taken out of the fit. The correlation coefficient improves then to 0.68 and 0.58 for H^N–N and H_α–C_α couplings, respectively. All correlation coefficients are summarized in Table 1. The fact that predicted and experimental RDCs match for the two domains indicates that the overall structure of the individual domains is preserved, but the relative orientation of the two domains of MalF-P2 is different in the crystal and in solution. This may be expected as the relative orientation of the two domains of MalF-P2 might change upon binding to MalE.

Interactions between MalF-P2 and MalE. To find out if and to what extent MalE can interact with the isolated P2 loop of MalF, we carried out isothermal titration calorimetry (ITC) experiments. Figure 4 shows that MalE and MalF-P2

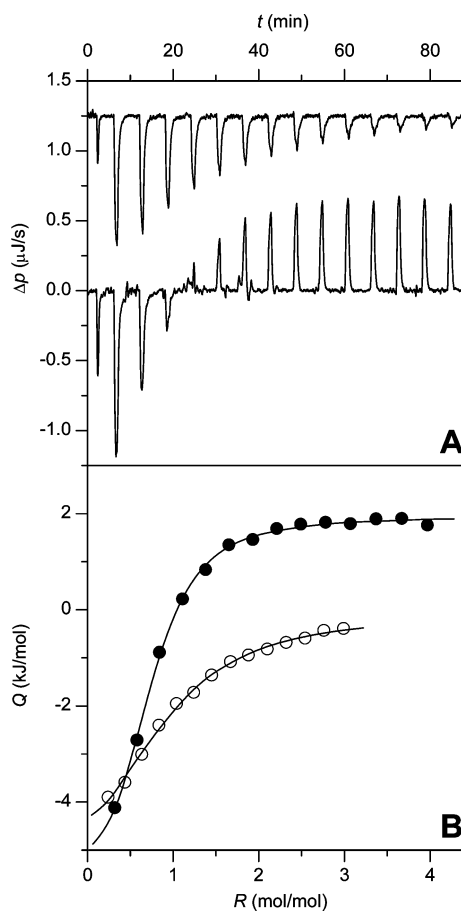


FIGURE 4: Isothermal titration calorimetry (ITC) curves obtained by titrating MalF-P2 with MalE. (A) Differential heating power, Δp , vs time t . ITC data were recorded at 5 °C in the absence (top) and presence (bottom) of maltose. One 5 μL and 14 20 μL aliquots of a concentrated MalE solution (667 μM in the absence of maltose, 885 μM in the presence of maltose) were injected into a 50 μM MalF-P2 solution in the absence (top trace) or presence (bottom trace) of 100 mM maltose. For the sake of clarity, the ITC curve obtained without maltose (top trace) was arbitrarily shifted along the ordinate by 1.25 $\mu\text{J/s}$. Constant endothermic peaks at the end of the titration with maltose (bottom trace) were due to dilution effects (most likely originating from slight differences in maltose concentration) and were also observed in control experiments in which MalE was injected into dialysis buffer containing 100 mM maltose but no P2 (data not shown). (B) Integrated and normalized heats of reaction, Q , vs MalE/P2 molar ratio, R . Fits (solid lines) to experimental data obtained in the absence (empty symbols) or presence (filled symbols) of 100 mM maltose yielded the following thermodynamic parameters characterizing the MalF-P2 interactions: $K_D = 22 \mu\text{M}$, $\Delta G^\circ = -24.9 \text{ kJ/mol}$, $\Delta H^\circ = -6.2 \text{ kJ/mol}$, and $T\Delta S^\circ = 18.6 \text{ kJ/mol}$ in the absence of maltose; $K_D = 7.4 \mu\text{M}$, $\Delta G^\circ = -27.3 \text{ kJ/mol}$, $\Delta H^\circ = -8.5 \text{ kJ/mol}$, and $T\Delta S^\circ = 18.8 \text{ kJ/mol}$ in the presence of 100 mM maltose. Initial 5 μL injections were excluded from the fitting procedure.

interact, even in the absence of other periplasmic loops of MalF and those of MalG. Assuming a 1:1 stoichiometry, fitting of the data yielded a dissociation constant (K_D) on the order of 10–20 μM , independent of the presence of maltose.

Binding of MalE to MalF-P2 in the absence of maltose ($K_D \approx 22 \mu\text{M}$) is only marginally weaker than in its presence ($K_D \approx 7.4 \mu\text{M}$). The endothermic peaks at the end of the titration performed in the presence of maltose are due to the heat of dilution. To confirm the interaction of purified MalF-P2 and MalE, we performed cross-linking experiments. A variant of MalF-P2 containing a mutation in domain 2

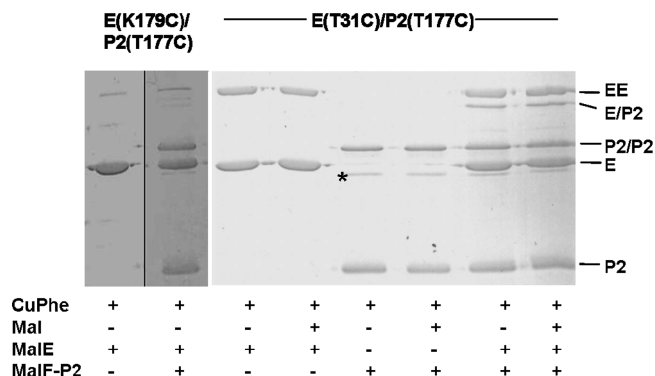


FIGURE 5: Site-specific CuPhe-induced cross-linking of the purified MalF P2 loop carrying a cysteine at position 177 with MalE(T31C) and MalE(K179C). MalF-P2 ($2.5 \mu\text{M}$) was incubated with the MalE variants ($2.5 \mu\text{M}$) and CuPhe in the absence or presence of maltose. The band marked with an asterisk is an impurity and is copurified only with the monocysteine variant of MalF-P2.

(T177C) was incubated with MalE(T31C) at a 1:1 molar ratio in the presence of CuPhe and subsequently analyzed for disulfide bond formation by SDS-PAGE. In the crystal structure, both residues are 5 Å apart and thus should readily form a disulfide bond. In fact, besides monomers and homodimers of both proteins, an additional band, comprising MalE and MalF-P2, could be observed (Figure 5) and verified by immunoblotting (data not shown). The product was found independent of the presence or absence of maltose, thereby confirming the results presented above. In contrast, only a faint band migrating at the size of a MalE-P2 cross-link could be detected when MalF-P2(T177C) was incubated with CuPhe in the presence of the MalE variant K179C (Figure 5). This residue is located in the hinge region of MalE and, according to the crystal structure, not within immediate cross-linking distance of MalF-P2(T177C). This result underscores the specificity of the MalF-P2–MalE interaction.

Additionally, the interaction between MalF-P2 and MalE was followed with site-specific resolution using solution-state NMR (Figure 6). We find that specific resonances display decreased intensities or are shifted if MalE is added to a solution of ^{15}N isotopically enriched MalF-P2. Spectra in the presence and absence of MalE were recorded under identical conditions (same buffer, without maltose). Similar chemical shift perturbations are observed in the presence of maltose. This behavior is expected as the dissociation constant of the binding is in the intermediate micromolar range. In case of strong binding, two separate sets of resonances are expected, reflecting the different chemical environment of bound and free MalF-P2. In the weak-binding limit, a continuous change in the $^1\text{H}-^{15}\text{N}$ chemical shifts of MalF-P2 as a function of the concentration of MalE would yield the dissociation constant of the interaction. In the case of intermediate binding, line broadening for those residues interacting with MalE occurs. At a MalF-P2:MalE molar ratio of 10:1, small perturbations of the chemical shifts are detected. Already at this low concentration of MalE, we find slightly reduced intensities of the MalF-P2 resonances. At a 1:1 molar ratio, the intensity of a large number of resonances is drastically reduced as a consequence of the interaction with MalE. Residues belonging to the C-terminal part and to the external loops of MalF-P2 remain largely unaffected by the binding process.

Strong interactions between MalF-P2 and MalE are also observed in the crystal structure of the MalFGK₂-E maltose transporter. Figure 7A summarizes the structural contacts observed in the crystal structure and the ones found in the NMR experiment. In the analysis of the X-ray contacts, all residues for which a heavy atom of MalF-P2 is within 5 Å of a heavy atom of MalE are taken into account. Residues which were selected as NMR interaction sites show a chemical shift change $\{[\delta\Delta(^1\text{H}) + \delta\Delta(^{15}\text{N})/5]^{1/2}\}$ larger than 0.03 ppm, which is equivalent to a ¹H shift change of 22.5 Hz at 750 MHz. Residues which are involved in the interaction are located in secondary structure elements $\alpha 1$ and $\beta 1$ (residues 100–110) and $\alpha 2$ and $\beta 6$ (residues 175–191), as well as in both linker region elements $\beta 1$ and $\beta 8$ which connect domains 1 and 2, including residues 112–116 and 200–208, respectively.

Figure 7B focuses on MalF-P2 (ribbon) and MalE (surface representation). For MalF-P2 residues which are colored orange and red, we find significant chemical shift perturbations indicating an involvement of those residues in binding to MalE. For residues that are colored blue, chemical shifts are unaffected upon addition of MalE. To probe if MalF-P2 is structurally reorganized upon binding to MalE, we repeated the RDC experiments in the presence of MalE. Figure 8 shows a correlation between experimental and theoretical RDC couplings for MalF-P2. The theoretical RDC values are again obtained by back-calculation from the X-ray structure of the maltose transporter using PALES (18). The correlation coefficient for domain 1 remains high, indicating that its structure is not perturbed upon addition of MalE. On the other hand, the correlation coefficient for domain 2 decreases significantly. This implies that the structure of domain 2 is different from the structure of domain 2 in the crystal. The overall correlation coefficient remains small ($R = 0.64$ for all amino acids, and $R = 0.64$ for full-length MalF-P2 without the C-terminal residues). Residues which are colored red (domain 2) are involved in crystal contacts with a MalK molecule in the symmetry-related unit cell in the X-ray structure.

DISCUSSION

We demonstrate in this work that the second periplasmic loop, P2, of MalF adopts a well-defined structure if over-produced individually and is not unfolded in solution (Figures 1 and 2). In that sense, MalF-P2 can be regarded as a receptor that recognizes MalE. The exceptional length of the second periplasmic loop in MalF is a particular property of enterobacteria (28). Deletion of this region impairs maltose transport. So far, however, it is not understood why enterobacteria require the extension of the loop. Given the fact that MalF-P2 has no stabilizing contacts to any protein component other than MalE in the X-ray structure of the maltose transporter, we can assume that the isolated MalF-P2 is a good model for studying the interactions between the maltose transporter and MalE. Analysis of RDC data shows that the structure of the two subdomains of MalF-P2 is similar in the crystal and in solution in the absence of MalE (Figure 3a,b). The relative orientation of the two domains of MalF-P2 is, however, different (Figure 3c). In NMR relaxation experiments, we find a correlation time for molecular tumbling (τ_C) of 8.4 ns. At this temperature and

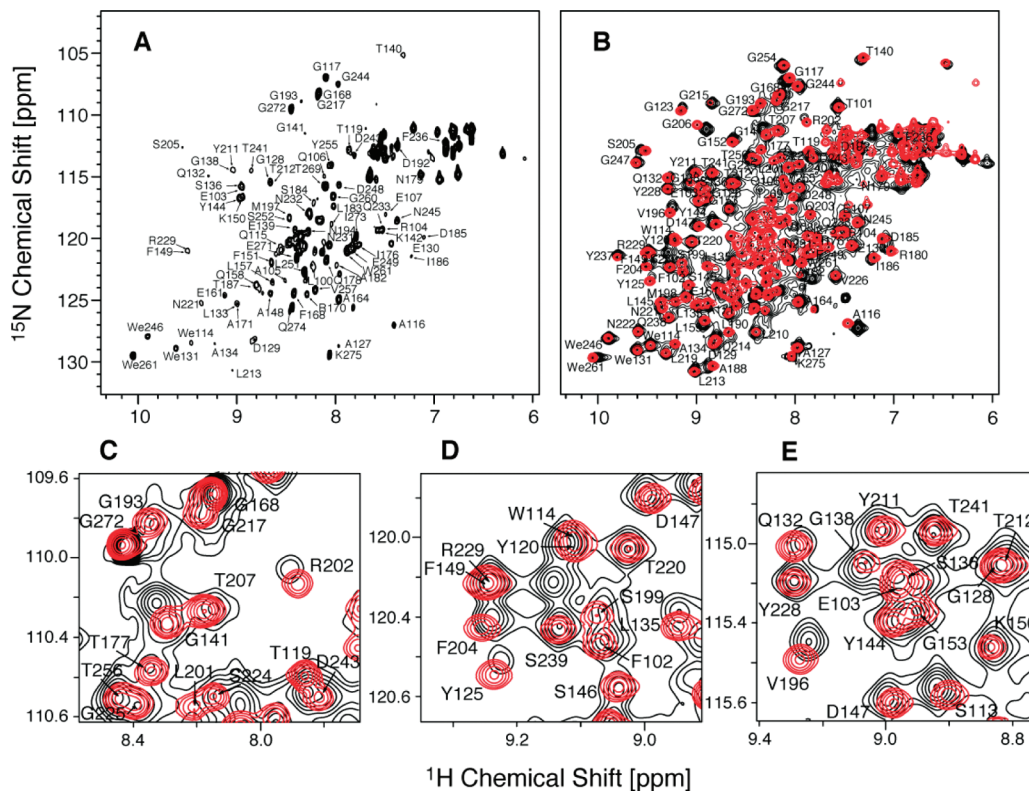


FIGURE 6: (A) ^1H - ^{15}N HSQC titration spectra of ^{15}N isotopically enriched MalF-P2 with MalE (1:1 molar ratio). (B) Superposition of MalF-P2 in the absence (red) and presence (black) of unlabeled MalE. In contrast to panel A, panel B is represented at lower contour levels. Panels C–E focus on particular spectral regions of the spectra represented in panel B.

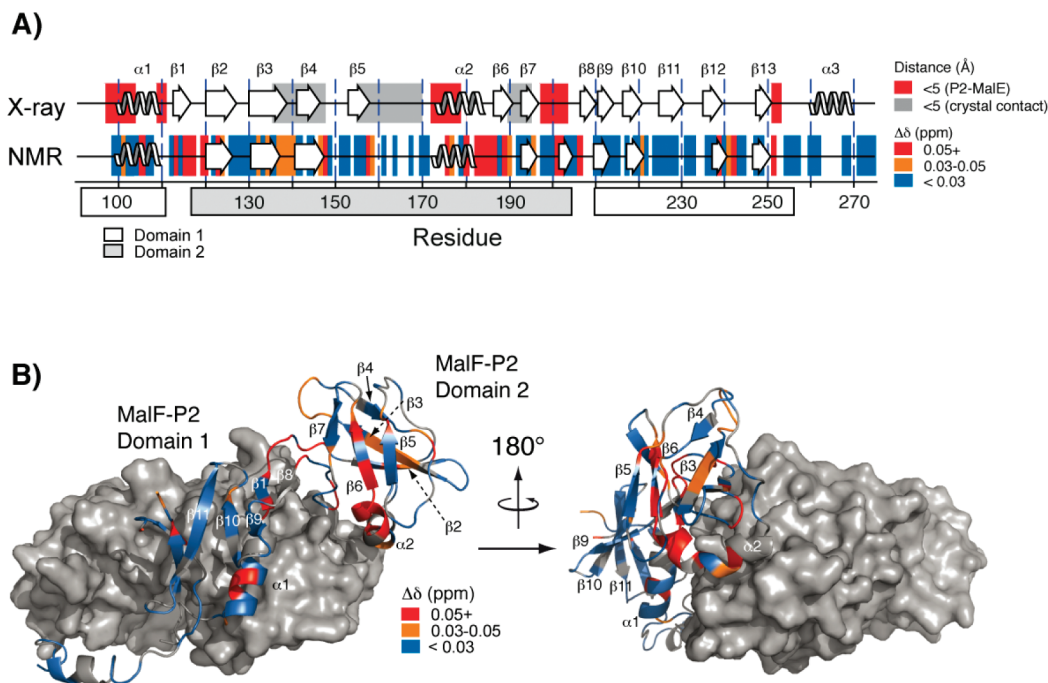


FIGURE 7: (A) Interactions between MalF-P2 and MalE, found in the crystal structure and as deduced from NMR chemical shift perturbations. In the analysis of the X-ray contacts, all residues in which a heavy atom of MalF-P2 is within 5 Å of a heavy atom of MalE (marked as red boxes) or MalK (marked as gray boxes) are taken into account. The analysis was carried out using CCP4i 1.3.20 (27). Sites of interaction between MalF-P2 and MalE are color-coded according to the size of the perturbation. (B) Structural representation of the residues of MalF-P2 which are experiencing chemical shift changes in the NMR experiment. MalE is drawn in surface representation.

protein concentration, this value of τ_C fits to a protein with a molecular mass of ~ 15 kDa. We explain this smaller than expected correlation time of the protein by assuming that the two domains of MalF-P2 can tumble independently of

each other and hence have a lower τ_C than one would have anticipated for a globular protein.

Merino et al. predicted that both conformations of MalE interact with the transporter (29). The authors showed that

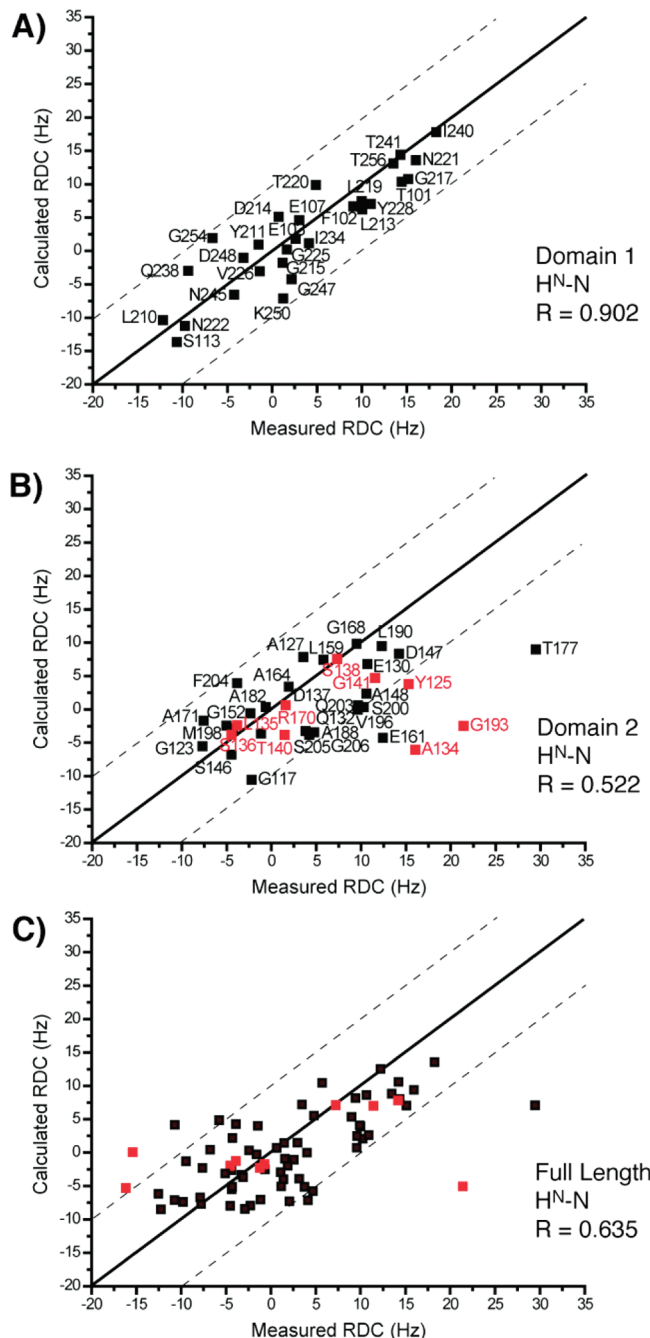


FIGURE 8: Experimental vs predicted RDC values for MalF-P2 in the presence of the maltose binding protein MalE. The theoretical RDC values are calculated from the X-ray structure using PALES (18). (A) RDC data fitted to domain 1 ($R = 0.90$), domain 2 ($R = 0.522$), and full-length MalF-P2 ($R = 0.64$) are represented in panels A–C, respectively. A lower correlation coefficient in the presence of MalE suggests that the conformations of domain 2 of MalF-P2 in the crystal structure and in solution are different. Residues which are colored red are involved in crystal contacts with a MalK molecule in the symmetry-related unit cell (see the Supporting Information).

unliganded MalE competes with liganded MalE in transport assays, and by fitting their data to theoretical equations, they concluded that maltose-free and maltose-bound MalE interact with the transporter with similar affinity. Both forms of the binding protein have access to the membrane components. Recent cross-linking experiments demonstrating the proximity of MalE(G13) to Pro78 in the first periplasmic loop of MalG in the presence and absence of maltose are consistent

with this notion (5). We find that MalF-P2 specifically binds to the maltose binding protein MalE in the presence and absence of substrate with similar affinity, even in the absence of MalG and the remaining part of MalF (Figure 4). The binding affinity is on the order of 10–20 μ M as determined by ITC experiments. From a structural point of view, it might be expected that the interaction between MalF-P2 and MalE is to first order independent of maltose as MalF-P2 binds to only one of the two domains of MalE. Our data are corroborated by the finding that the isolated P2 loop carrying a cysteine residue at position 177 cross-links to MalE(T31C) in the absence or presence of maltose (Figure 5). Previous biochemical experiments revealed that a MalE concentration of 25–100 μ M is required to maintain half-maximal transport rates (30, 31). This is in agreement with EPR studies in which 60% of MalE was bound to MalFGK₂ at protein concentrations of 50–100 μ M (32). Together, our findings are consistent with cross-linking data, demonstrating MalE–MalF-P2 interaction throughout the transport cycle in the context of the assembled MalFGK₂ complex (33).

Upon titration of MalE with MalF-P2, most of the NMR resonances show decreased intensities and a specific subset displays significant chemical shift changes (Figure 6), indicating that the amino acids associated with these resonances are involved in MalE binding. An interaction of MalE with the integral membrane components MalF and MalG was observed previously in the crystal structure of the catalytic intermediate state of the maltose transporter (3), in which the N-terminal lobe of MalE interacts with MalF (MalF-P2). The C-terminal lobe of MalE binds mostly to periplasmic loop P3 of MalG. From the NMR titration experiments, we find that the amino acids that are involved in the interaction between MalF-P2 and MalE are localized in domain 1, containing secondary structure elements α 1 and β 1 (residues 100–110), in domain 2 α 2 and β 6 (residues 175–191), and both linker regions β 1 and β 8 which connect domains 1 and 2, including residues 112–116 and 200–208, respectively. This is in agreement with the X-ray structure in which a similar interaction interface is found (Figure 7). The assumption that the MalFGK₂ complex must be able to attain at least two different conformations in its interaction with MalE, only one of which is able to trigger ATP hydrolysis by MalK (2, 34), is confirmed by EPR data (32, 35). Davidson and co-workers found that there was no change in affinity of MalE for MalFGK₂ in its substrate-free or substrate-bound form. This is in agreement with our ITC binding data which show that MalF-P2 interacts with MalE similarly in the presence and absence of substrate.

The fitting of H^N-N residual dipolar couplings of MalF-P2 bound to MalE yields the correlation coefficients (R) of 0.90 for domain 1, 0.52 for domain 2, and 0.64 for all residues of MalF-P2 (Figure 8). The correlation coefficient is invariant to a truncation of the C-terminus in the analysis ($R = 0.64$). All correlation coefficients determined for free MalF-P2 and MalF-P2 after addition of MalE are summarized in Table 1. In the bound state, the high correlation coefficient which is observed for domain 1 indicates that the overall structure of this domain is comparable to its structure in the unbound state. Most of the outliers in the correlation plot belong to regions of MalF-P2 at the surface of the structure, predominantly in domain 2 of MalF-P2. There, the conformation might be

perturbed due to crystal packing effects and/or dynamic effects. Indeed, we find a number of contacts between domain 2 of MalF-P2 and the MalK subunits of the symmetry-related maltose transporter in the crystal (see the Supporting Information). These residues are colored red in Figure 8. Crystal contacts might induce local structural perturbations which in turn affect the local conformation of the protein in domain 2. Apparently, domain 2 of MalF-P2 interacts preferably with a MalK molecule in a symmetry-related unit cell, such that the X-ray structure of domain 2 of MalF-P2 resembles more the structure in the unbound state.

To summarize, we find that individually expressed MalF-P2 represents a well-folded membrane protein receptor to which the maltose binding protein MalE is bound in the presence and absence of maltose. The structures of the two individual domains of MalF-P2 in the absence of MalE are comparable to the conformation found in the X-ray structure. Upon titration of MalE with MalF-P2, the two domains of MalF-P2 change their relative orientation to accommodate the ligand. Under these conditions, a conformational change of domain 2 of MalF-P2 is induced, resulting in a structure which is distinct from the conformation found in the X-ray structure. We assume that crystal contacts between MalF-P2 and MalK are the reason for differences in conformation observed in the crystal and in solution.

ACKNOWLEDGMENT

We thank Dr. Katja Faelber for assistance in the analysis of crystallographic data.

SUPPORTING INFORMATION AVAILABLE

NMR titration plots, analytical ultracentrifugation data for MalF-P2, structural representation of crystallographic contacts between maltose transporters in symmetry-related unit cells (Protein Data Bank entry 2R6G), and H^N-N and H α -C α RDC values for MalF-P2 in the presence and absence of MalE. This material is available free of charge via the Internet at <http://pubs.acs.org>.

REFERENCES

- Higgins, C. F. (1992) ABC Transporters: From Microorganisms to Man. *Annu. Rev. Cell Biol.* 8, 67–113.
- Boos, W., and Lucht, J. M. (1996) *Periplasmic binding protein-dependant ABC transporters in E. coli and Salmonella typhimurium: Cellular and molecular biology* (Neidhardt, F. C., Curtiss, R., Ingraham, J. L., Lin, E. C. C., Low, K. B., and Magasanik, B., Eds.) pp 1175–1209, American Society for Microbiology Press, Washington, DC.
- Oldham, M. L., Khare, D., Quiocho, F. A., Davidson, A. L., and Chen, J. (2007) Crystal structure of a catalytic intermediate of the maltose transporter. *Nature* 450, 515–522.
- Hor, L. I., and Shuman, H. A. (1993) Genetic-analysis of periplasmic binding-protein dependent transport in *Escherichia Coli*: Each lobe of maltose-binding protein interacts with a different subunit of the MalFGK₂ membrane-transport complex. *J. Mol. Biol.* 233, 659–670.
- Daus, M. L., Berendt, S., Wuttge, S., and Schneider, E. (2007) Maltose binding protein (MalE) interacts with periplasmic loops P2 and P1 respectively of the MalFG subunits of the maltose ATP binding cassette transporter (MalFGK₂) from *Escherichia coli* and *Salmonella* during the transport cycle. *Mol. Microbiol.* 66, 1107–1122.
- Froshauer, S., Green, G. N., Boyd, D., McGovern, K., and Beckwith, J. (1988) Genetic Analysis of the Membrane Insertion and Topology of MalF, a Cytoplasmic Membrane Protein of *Escherichia coli*. *J. Mol. Biol.* 200, 501–511.
- Daus, M. L., Grote, M., Müller, P., Doepper, M., Herrmann, A., Steinhof, H.-J., Dassa, E., and Schneider, E. (2007) ATP-driven MalK dimer closure and re-opening and conformational changes of the ‘EAA’ motifs are crucial for function of the maltose ATP-binding cassette transporter (MalFGK₂). *J. Biol. Chem.* 282, 22387–22369.
- Yang, D., Venters, R. A., Mueller, G. A., Choy, W. Y., and Kay, L. E. (1999) TROSY-based HNCO pulse sequence for the measurement of ¹HN-¹⁵N, ¹⁵N-¹³CO, ¹HN-¹³CO, ¹³CO-¹³C and ¹HN-¹³C dipolar couplings in ¹⁵N, ¹³C, ²H labeled proteins. *J. Biomol. NMR* 14, 333–343.
- Sattler, M., Schleucher, J., and Griesinger, C. (1999) Heteronuclear multidimensional NMR experiments for the structure determination of proteins in solution employing pulsed field gradients. *Prog. NMR Spectrosc.* 34, 93–158.
- Cavanagh, J., Fairbrother, W. J., Palmer, A. G., and Skelton, N. J. (1996) *Protein NMR Spectroscopy: Principles and Practice*, Academic Press, San Diego.
- Gryk, M. R., Abeßer, R., Simon, B., Nilges, M., and Oschkinat, H. (1988) Heteronuclear relaxation study of the PH domain of β -spectrin: Restriction of loop motions upon binding inositol trisphosphate. *J. Mol. Biol.* 280, 879–896.
- Dayie, K. T., Wagner, G., and Lefèvre, J. F. (1996) Theory and Practice of Nuclear Spin Relaxation in Proteins. *Annu. Rev. Phys. Chem.* 47, 243–282.
- Ottiger, M., Delaglio, F., and Bax, A. (1998) Measurement of J and dipolar couplings from simplified two-dimensional NMR spectra. *J. Magn. Reson.* 131, 373–378.
- Bax, A., Kontaxis, G., and Tjandra, N. (2001) Dipolar couplings in macromolecular structure determination. *Methods Enzymol.* 339, 127–174.
- Vranken, W. F., Boucher, W., Stevens, T. J., Pajon, R. F. A., Llinas, M. L., Ulrich, E., Markley, J. L., Ionides, J., and Laue, E. D. (2005) The CCPN Data Model for NMR Spectroscopy: Development of a Software Pipeline. *Proteins* 59, 687–696.
- Venters, R. A., Farmer, B. T., Fierke, C. A., and Spicer, L. D. (1996) Characterizing the use of perdeuteration in NMR studies of large proteins C-13, N-15 and H-1 assignments of human carbonic anhydrase II. *J. Mol. Biol.* 264, 1101–1116.
- Cornilescu, G., Delaglio, F., and Bax, A. (1999) Protein backbone angle restraints from searching a database for chemical shift and sequence homology. *J. Biomol. NMR* 13, 289–302.
- Zweckstetter, M., and Bax, A. (2000) Prediction of Sterically Induced Alignment in a Dilute Liquid Crystalline Phase: Aid to Protein Structure Determination by NMR. *J. Am. Chem. Soc.* 122, 3791–3792.
- Wiseman, T., Williston, S., Brandts, J. F., and Lin, L.-N. (1989) Rapid measurement of binding constants and heats of binding using a new titration calorimeter. *Anal. Biochem.* 179, 131–137.
- Navaza, J. (1994) The CCP4 Suite: Programs for Protein Crystallography. *Acta Crystallogr. A50*, 157–163.
- DeLano, W. L. (2002) PyMol, DeLano Scientific, San Carlos, CA.
- Jacso, T., Grote, M., Schmieder, P., Schneider, E., and Reif, B. (2008) NMR assignments of the periplasmic loop P2 of the MalF subunit of the maltose ATP binding cassette transporter. *Biomol. NMR Assign.* doi: 10.1007/s12104-008-9131-7.
- Tjandra, N., and Bax, A. (1997) Direct Measurement of Distances and Angles in Biomolecules by NMR in a Dilute Liquid Crystalline Medium. *Science* 278, 1111–1114.
- Prestegard, J. H., Al-Hashimi, H. M., and Tolman, J. R. (2000) NMR structures of biomolecules using field oriented media and residual dipolar couplings. *Q. Rev. Biophys.* 33, 371–424.
- Hansen, M. R., Mueller, L., and Pardi, A. (1998) Tunable Allignment of Macromolecules by filamentous phage yields dipolar coupling interactions. *Nat. Struct. Biol.* 5, 1065–1074.
- Hansen, M. R., Hanson, P., and Pardi, A. (2000) Filamentous bacteriophage for aligning RNA, DNA, and proteins for measurement of nuclear magnetic resonance dipolar coupling interactions. *Methods Enzymol.* 317, 220–240.
- Collaborative Computational Project Number 4 (1994) The CCP4 Suite: Programs for Protein Crystallography. *Acta Crystallogr. D50*, 760–763.
- Tapia, M. I., Mourez, M., Hofnung, M., and Dassa, E. (1999) Structure-function study of MalF protein by random mutagenesis. *J. Bacteriol.* 181, 2267–2272.
- Merino, G., Boos, W., Shuman, H. A., and Bohl, E. (1995) The inhibitor of maltose transport by the unliganded form of the

- maltose-binding protein of *E. coli*: Experimental findings and mathematical treatment. *J. Theor. Biol.* 177, 171–179.
30. Dean, D. A., Hor, L. I., Shuman, H. A., and Nikaido, H. (1992) Interaction between Maltose-Binding Protein and the Membrane-associated Maltose Transporter Complex in *Escherichia coli*. *Mol. Microbiol.* 6, 2033–2040.
31. Manson, M. D., Boos, W., Bassford, P. J. J., and Rasmussen, B. A. (1985) Dependence of Maltose Transport and Chemotaxis on the Amount of Maltose-Binding Protein. *J. Biol. Chem.* 260, 9727–9733.
32. Austermuhle, M. I., Hall, J. A., Klug, C. S., and Davidson, A. L. (2004) Maltose-binding Protein Is Open in the Catalytic Transition State for ATP Hydrolysis during Maltose Transport. *J. Biol. Chem.* 279, 28243–28250.
33. Daus, M. L., Grote, M., and Schneider, E. (2009) The MalF-P2 loop of the ATP-binding cassette (ABC) transporter MalFGK2 from *Escherichia coli/Salmonella enterica* serovar Typhimurium interacts with maltose binding protein (MalE) throughout the catalytic cycle. *J. Bacteriol.* . doi: 10.1128/JB.01439-08.
34. Shilton, B. H., Shuman, H. A., and Mowbray, S. L. (1996) Crystal structures and solution conformations of a dominant-negative mutant of *E. coli* maltose-binding protein. *J. Mol. Biol.* 264, 364–376.
35. Davidson, A. L., and Chen, J. (2004) ATP-binding cassette transporters in bacteria. *Annu. Rev. Biochem.* 73, 241–268.

BI801376M

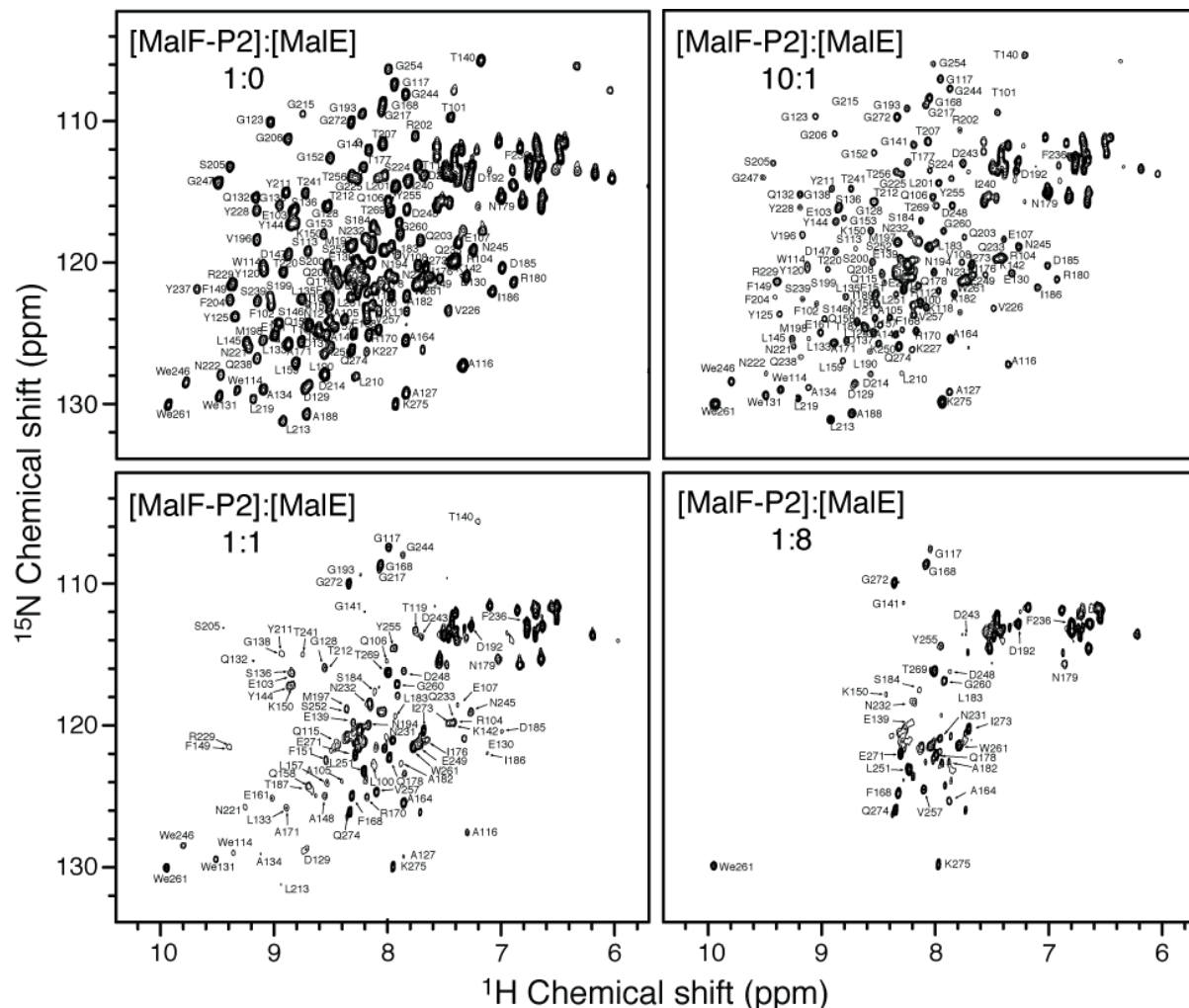
Supporting Information for the manuscript

The periplasmic loop P2 of the MalF subunit of the maltose ATP binding cassette transporter is sufficient to bind the maltose binding protein MalE

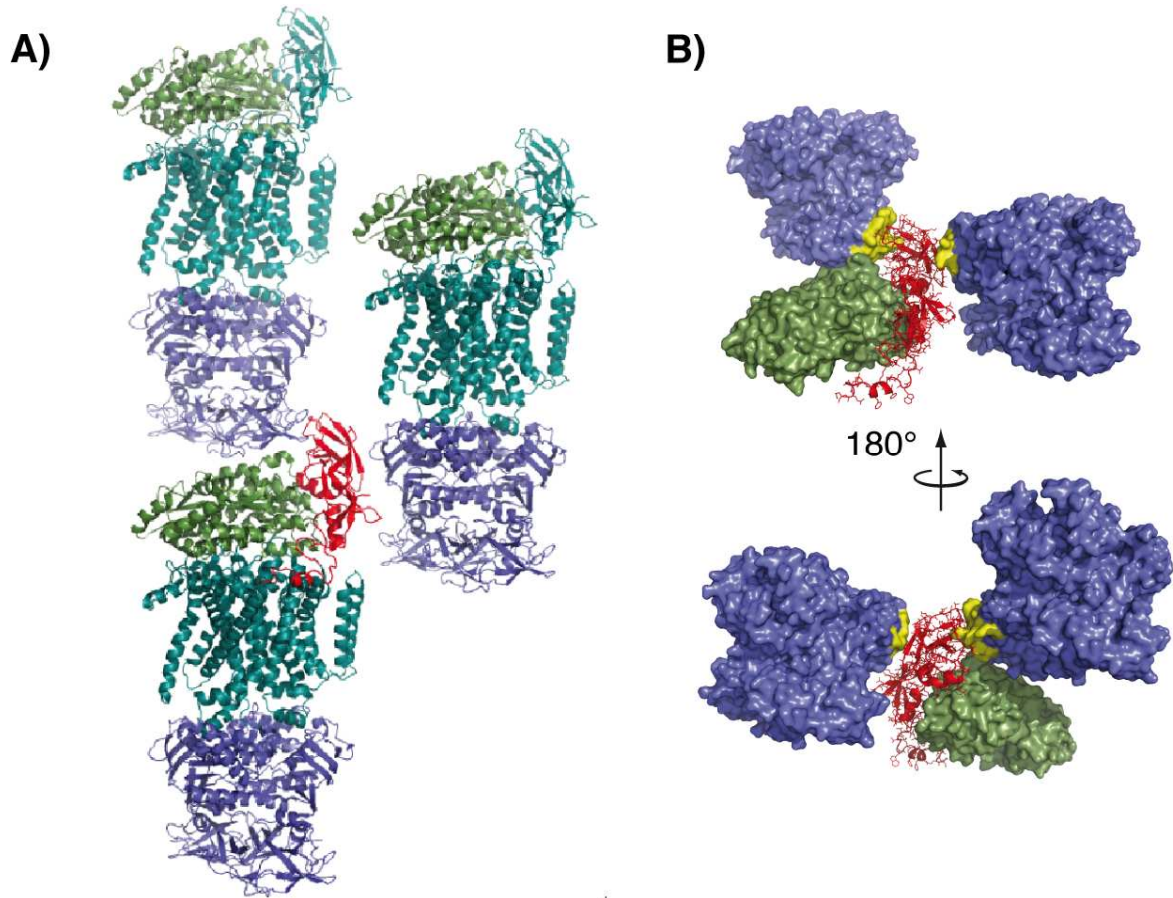
by

Tomas Jacso, Mathias Grote, Martin L. Daus, Peter Schmieder, Sandro Keller,

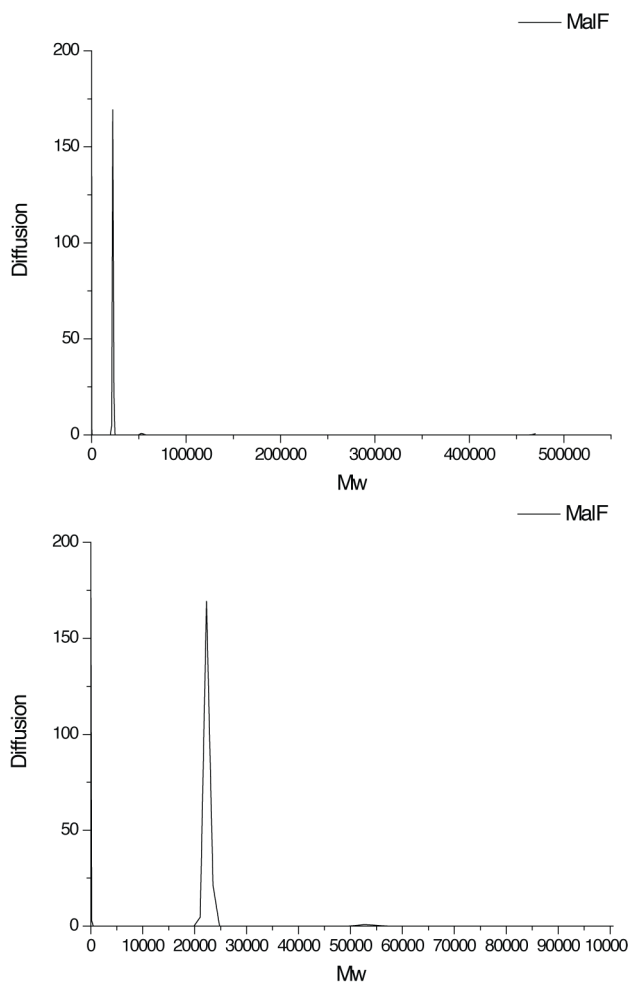
Erwin Schneider and Bernd Reif



Supporting Figure 1. ^1H - ^{15}N correlation spectrum of MalF-P2 upon titration of MalE. The ratio of the respective protein concentrations is indicated in the figure.



Supporting Figure 2. Crystal contacts in the X-ray structure of MalFGK₂·MalE (PDB: 2R6G). MalF, MalG are drawn in dark green, MalE in light green, MalK in blue, respectively. The periplasmic loop P2 of MalF is represented in red. In particular, the second domain of MalF-P2 has many intermolecular contacts to a MalK molecule in a neighboring unit cell. Crystal contacts between MalF-P2 and MalK effects only the second domain of MalF-P2, namely the residues N121, Y125, A134, L135, S136, S138, E139, T140, G141, N143, Y144, L145, D147, E154, Q155, K156, Q158, T163, Q165, E169, R170, I189, G193, K195 (indicated in yellow in panel B).



Supporting Figure 3. Analytical Ultracentrifugation demonstrates MalF-P2 is monomeric at the concentration used in this study. The continuous sedimentation distribution $c(s)$ after maximum entropy regularization yields only one sharp peak. After transformation to a molar mass distribution and an area determination of all peaks in the spectrum, we find only monomeric MalF-P2 (the peak at 21 kDa accounts for 98% of the total area for the experiment). Top, shows full molecular weight sampling to confirm that no high order oligomers are present. Bottom, shows the enlarged peak to verify the apparent molecular mass.

Supporting Table 1. RDCs for MalF-P2 in absence and presence of MalE (ratio= 1:1)

All residues are listed according to the full length MalF primary sequence, specifying residue type, nucleus, the observed residual dipolar coupling (D_{OBS}), the back calculated residual coupling (D) using the PDB file 2R6G, and the difference in coupling (D_{DIFF}), respectively.

HnN all (in absence of MalE)

ID_I	RES_I	ATOM_I	ID_J	RES_J	ATOM_J	D_{OBS}	D	D_{DIFF}
100	LEU	H	100	LEU	N	1,6442	1,399	0,2452
101	THR	H	101	THR	N	4,9807	7,409	-2,4283
102	PHE	H	102	PHE	N	3,0967	5,8073	-2,7106
105	ALA	H	105	ALA	N	4,6432	7,0907	-2,4475
106	GLN	H	106	GLN	N	-5,8213	3,8872	-9,7085

107	GLU	H	107	GLU	N	4,3539	0,6023	3,7517
113	SER	H	113	SER	N	-2,486	-12,4556	9,9696
115	GLN	H	115	GLN	N	-8,6411	-4,0782	-4,563
116	ALA	H	116	ALA	N	-2,35	4,3388	-6,6888
117	GLY	H	117	GLY	N	-9,9317	-1,4718	-8,4599
118	LYS	H	118	LYS	N	-16,7989	0,2217	-17,0206
119	THR	H	119	THR	N	12,2509	1,4141	10,8367
121	ASN	H	121	ASN	N	12,3275	7,9805	4,347
123	GLY	H	123	GLY	N	-22,1468	-12,7176	-9,4292
125	TYR	H	125	TYR	N	-16,3551	-4,4753	-11,8798
127	ALA	H	127	ALA	N	13,2139	6,808	6,4059
130	GLU	H	130	GLU	N	14,7357	6,0044	8,7313
132	GLN	H	132	GLN	N	-19,6447	-12,5685	-7,0762
134	ALA	H	134	ALA	N	-11,3373	-8,8226	-2,5147
135	LEU	H	135	LEU	N	-12,869	-5,8793	-6,9897
137	ASP	H	137	ASP	N	-6,3875	-4,2783	-2,1092
140	THR	H	140	THR	N	11,2755	3,8863	7,3892
141	GLY	H	141	GLY	N	-1,3079	3,0544	-4,3624
144	TYR	H	144	TYR	N	-18,5234	-11,0397	-7,4837
145	LEU	H	145	LEU	N	-13,9284	-9,7568	-4,1717
147	ASP	H	147	ASP	N	5,9944	3,9181	2,0763
148	ALA	H	148	ALA	N	-9,1381	-1,1026	-8,0355
150	LYS	H	150	LYS	N	-12,4042	-8,7	-3,7041
151	PHE	H	151	PHE	N	-0,6638	3,9663	-4,6302
152	GLY	H	152	GLY	N	9,4855	0,8268	8,6587
153	GLY	H	153	GLY	N	-23,7007	-11,7252	-11,9755
156	LYS	H	156	LYS	N	-0,7281	-7,5654	6,8372
157	LEU	H	157	LEU	N	-2,2549	-3,2204	0,9655
158	GLN	H	158	GLN	N	7,9006	0,4236	7,4771
159	LEU	H	159	LEU	N	14,6343	8,9126	5,7217
161	GLU	H	161	GLU	N	-14,1163	-10,1008	-4,0155
164	ALA	H	164	ALA	N	0,2905	-3,0564	3,3469
168	GLY	H	168	GLY	N	5,443	6,4265	-0,9835
170	ALA	H	170	ALA	N	14,2424	3,2703	10,9721
177	THR	H	177	THR	N	-2,376	2,9003	-5,2763
178	GLN	H	178	GLN	N	9,9985	6,2902	3,7083
179	ASN	H	179	ASN	N	9,7574	1,5141	8,2433
180	ARG	H	180	ARG	N	-16,6172	-9,9236	-6,6936
182	ALA	H	182	ALA	N	-11,6451	-0,7837	-10,8614
183	LEU	H	183	LEU	N	-21,902	-9,6971	-12,2048
184	SER	H	184	SER	N	-11,9678	-1,6085	-10,3592
185	ASP	H	185	ASP	N	-0,1038	3,6474	-3,7512
186	ILE	H	186	ILE	N	-14,0125	-9,6507	-4,3618
188	ALA	H	188	ALA	N	-7,0637	-11,5273	4,4635
190	LEU	H	190	LEU	N	7,018	8,7165	-1,6985
192	ASP	H	192	ASP	N	-14,2474	-12,4358	-1,8116
193	GLY	H	193	GLY	N	-1,7196	-9,4351	7,7156
196	VAL	H	196	VAL	N	1,7319	2,4846	-0,7527
198	MET	H	198	MET	N	3,9967	0,2921	3,7046
199	SER	H	199	SER	N	3,5282	7,2941	-3,7659
200	SER	H	200	SER	N	-2,0286	-2,4359	0,4073
201	LEU	H	201	LEU	N	-11,4214	-6,3136	-5,1078
204	PHE	H	204	PHE	N	6,144	5,5754	0,5686
205	SER	H	205	SER	N	11,6253	3,1886	8,4367
206	GLY	H	206	GLY	N	3,5207	1,9849	1,5358
210	LEU	H	210	LEU	N	7,6423	-8,9916	16,6339

211	TYR	H	211	TYR	N	8,2085	1,9341	6,2744
213	LEU	H	213	LEU	N	12,2088	5,2582	6,9507
214	ASP	H	214	ASP	N	2,24	3,6615	-1,4215
217	GLY	H	217	GLY	N	8,3815	3,3681	5,0134
219	LEU	H	219	LEU	N	3,3637	-1,4318	4,7955
220	THR	H	220	THR	N	-5,9808	7,4331	-13,4139
221	ASN	H	221	ASN	N	8,6906	8,875	-0,1844
222	ASN	H	222	ASN	N	10,2086	-9,517	19,7256
227	LYS	H	227	LYS	N	11,6142	3,5574	8,0568
228	TYR	H	228	TYR	N	2,4205	3,1836	-0,7631
232	ASN	H	232	ASN	N	4,3181	-10,8672	15,1853
237	TYR	H	237	TYR	N	-6,207	-0,5896	-5,6174
238	GLN	H	238	GLN	N	-16,1969	3,4578	-19,6547
239	SER	H	239	SER	N	-9,0268	-5,4658	-3,561
240	ILE	H	240	ILE	N	13,9902	8,8514	5,1388
241	THR	H	241	THR	N	7,6287	6,3705	1,2582
245	ASN	H	245	ASN	N	-1,5354	1,17	-2,7054
247	GLY	H	247	GLY	N	-5,5358	1,7004	-7,2362
248	ASP	H	248	ASP	N	8,8414	-4,0543	12,8957
250	LYS	H	250	LYS	N	-13,4512	-2,9645	-10,4867
254	GLY	H	254	GLY	N	-5,2428	-4,1479	-1,0949
255	TYR	H	255	TYR	N	4,2847	2,419	1,8657
257	VAL	H	257	VAL	N	-8,3383	-3,4069	-4,9314
260	GLY	H	260	GLY	N	10,7303	6,9451	3,7853
268	PHE	H	268	PHE	N	-1,4105	-6,7218	5,3113
269	THR	H	269	THR	N	-2,8655	6,6277	-9,4932
271	GLU	H	271	GLU	N	1,8345	-10,4089	12,2434
272	GLY	H	272	GLY	N	-4,2452	1,5758	-5,821
273	ILE	H	273	ILE	N	-8,9972	-11,4639	2,4667
274	GLN	H	274	GLN	N	2,2227	-6,3628	8,5855
275	LYS	H	275	LYS	N	3,606	-1,0318	4,6379

HnN domain 1 (in absence of MalE)

ID_I	RES_I	ATOM_I	ID_J	RES_J	ATOM_J	D_OBS	D	D_DIFF
100	LEU	H	100	LEU	N	1,6442	-1,449	3,0939
101	THR	H	101	THR	N	4,9807	6,688	-1,7075
102	PHE	H	102	PHE	N	3,0967	-0,3	3,3971
105	ALA	H	105	ALA	N	4,6432	0,32	4,3226
106	GLN	H	106	GLN	N	-5,8213	-1,012	-4,8085
107	GLU	H	107	GLU	N	4,3539	5,386	-1,032
113	SER	H	113	SER	N	-2,486	-0,427	-2,0583
210	LEU	H	210	LEU	N	7,6423	6,801	0,8404
211	TYR	H	211	TYR	N	8,2085	6,779	1,4287
213	LEU	H	213	LEU	N	12,2088	6,665	5,5438
214	ASP	H	214	ASP	N	2,24	-2,7	4,9403
217	GLY	H	217	GLY	N	8,3815	6,265	2,1163
219	LEU	H	219	LEU	N	3,3637	6,163	-2,7992
220	THR	H	220	THR	N	-5,9808	5,774	11,7551
221	ASN	H	221	ASN	N	8,6906	6,416	2,2741
222	ASN	H	222	ASN	N	10,2086	5,564	4,6445
227	LYS	H	227	LYS	N	11,6142	6,546	5,0674
228	TYR	H	228	TYR	N	2,4205	-1,152	3,5728
232	ASN	H	232	ASN	N	4,3181	-5,392	9,7104
237	TYR	H	237	TYR	N	-6,207	-1,556	-4,6509
238	GLN	H	238	GLN	N	-16,1969	-9,749	-6,4472
239	SER	H	239	SER	N	-9,0268	-8,655	-0,371
240	ILE	H	240	ILE	N	13,9902	6,531	7,4588
241	THR	H	241	THR	N	7,6287	5,977	1,6515
245	ASN	H	245	ASN	N	-1,5354	-12,502	10,9666
247	GLY	H	247	GLY	N	-5,5358	-2,289	-3,2467
248	ASP	H	248	ASP	N	8,8414	6,689	2,1523
250	LYS	H	250	LYS	N	-13,4512	-11,518	-1,9324
254	GLY	H	254	GLY	N	-5,2428	0,38	-5,6234
255	TYR	H	255	TYR	N	4,2847	6,527	-2,2432
257	VAL	H	257	VAL	N	-8,3383	-7,067	-1,2709

HnN domain 2 (in absence of MalE)

ID_I	RES_I	ATOM_I	ID_J	RES_J	ATOM_J	D_OBS	D	D_DIFF
117	GLY	H	117	GLY	N	-9,9317	-4,6545	-5,2772
118	LYS	H	118	LYS	N	-16,7989	4,891	-21,6899
119	THR	H	119	THR	N	12,2509	6,0901	6,1608
121	ASN	H	121	ASN	N	12,3275	9,3748	2,9527
123	GLY	H	123	GLY	N	-22,1468	-18,4973	-3,6495
125	TYR	H	125	TYR	N	-16,3551	-5,6973	-10,6578
127	ALA	H	127	ALA	N	13,2139	10,9815	2,2324
130	GLU	H	130	GLU	N	14,7357	7,3626	7,373
132	GLN	H	132	GLN	N	-19,6447	-16,8172	-2,8275
134	ALA	H	134	ALA	N	-11,3373	-14,6164	3,279
135	LEU	H	135	LEU	N	-12,869	-9,7998	-3,0692
137	ASP	H	137	ASP	N	-6,3875	-6,2594	-0,1281
140	THR	H	140	THR	N	11,2755	7,3357	3,9398
141	GLY	H	141	GLY	N	-1,3079	2,6495	-3,9574
144	TYR	H	144	TYR	N	-18,5234	-17,1347	-1,3887
145	LEU	H	145	LEU	N	-13,9284	-16,8456	2,9172
147	ASP	H	147	ASP	N	5,9944	3,2195	2,7749
148	ALA	H	148	ALA	N	-9,1381	-2,7661	-6,372
150	LYS	H	150	LYS	N	-12,4042	-10,9012	-1,503
151	PHE	H	151	PHE	N	-0,6638	0,9086	-1,5724
152	GLY	H	152	GLY	N	9,4855	5,4403	4,0452
153	GLY	H	153	GLY	N	-23,7007	-17,1672	-6,5335
156	LYS	H	156	LYS	N	-0,7281	-4,6977	3,9696
157	LEU	H	157	LEU	N	-2,2549	-1,329	-0,9258
158	GLN	H	158	GLN	N	7,9006	4,5397	3,3609
159	LEU	H	159	LEU	N	14,6343	8,6786	5,9557
161	GLU	H	161	GLU	N	-14,1163	-16,2032	2,0869
164	ALA	H	164	ALA	N	0,2905	1,2948	-1,0043
168	GLY	H	168	GLY	N	5,443	10,7368	-5,2938
170	ALA	H	170	ALA	N	14,2424	8,9963	5,2461
177	THR	H	177	THR	N	-2,376	3,4239	-5,7999
178	GLN	H	178	GLN	N	9,9985	10,0733	-0,0748
179	ASN	H	179	ASN	N	9,7574	7,8038	1,9536
180	ARG	H	180	ARG	N	-16,6172	-17,4771	0,8599
182	ALA	H	182	ALA	N	-11,6451	-5,6594	-5,9857
183	LEU	H	183	LEU	N	-21,902	-17,3524	-4,5496
184	SER	H	184	SER	N	-11,9678	-5,7701	-6,1977
185	ASP	H	185	ASP	N	-0,1038	0,1629	-0,2668
186	ILE	H	186	ILE	N	-14,0125	-14,2543	0,2418
188	ALA	H	188	ALA	N	-7,0637	-14,7941	7,7304
190	LEU	H	190	LEU	N	7,018	10,1032	-3,0852
192	ASP	H	192	ASP	N	-14,2474	-17,3758	3,1284
193	GLY	H	193	GLY	N	-1,7196	-14,5501	12,8306
196	VAL	H	196	VAL	N	1,7319	5,8864	-4,1545
198	MET	H	198	MET	N	3,9967	6,418	-2,4213
199	SER	H	199	SER	N	3,5282	11,022	-7,4939
200	SER	H	200	SER	N	-2,0286	-5,0335	3,0049
201	LEU	H	201	LEU	N	-11,4214	-7,7423	-3,679
204	PHE	H	204	PHE	N	6,144	8,7123	-2,5683
205	SER	H	205	SER	N	11,6253	7,046	4,5793
206	GLY	H	206	GLY	N	3,5207	7,8104	-4,2896

HaCa all (in absence of MalE)

ID_I	RES_I	ATOM_I	ID_J	RES_J	ATOM_J	D_OBS	D	D_DIFF
99	GLN	HA	99	GLN	CA	-0,55	-2,6279	2,0778
100	LEU	HA	100	LEU	CA	-1,0142	-0,1645	-0,8498
101	THR	HA	101	THR	CA	-33,8123	-16,6767	-17,1356
102	PHE	HA	102	PHE	CA	31,6103	1,8728	29,7375
103	GLU	HA	103	GLU	CA	-24,5175	18,7854	-43,3029
104	ARG	HA	104	ARG	CA	-8,5401	-11,6003	3,0602
105	ALA	HA	105	ALA	CA	20,0587	2,7228	17,3359
106	GLN	HA	106	GLN	CA	14,0036	-0,3612	14,3649
107	GLU	HA	107	GLU	CA	-12,8432	20,7727	-33,6159
108	VAL	HA	108	VAL	CA	-28,3592	-18,0872	-10,272
112	ARG	HA	112	ARG	CA	-28,8951	14,9721	-43,8671
113	SER	HA	113	SER	CA	3,5228	22,137	-18,6141
114	TRP	HA	114	TRP	CA	6,4419	21,3624	-14,9206
115	GLN	HA	115	GLN	CA	14,5782	7,4688	7,1094
118	LYS	HA	118	LYS	CA	-3,6559	12,6831	-16,3389
119	THR	HA	119	THR	CA	-42,7336	-2,4737	-40,2599
120	TYR	HA	120	TYR	CA	-48,7038	-4,2012	-44,5026
121	ASN	HA	121	ASN	CA	10,9497	2,091	8,8587
127	ALA	HA	127	ALA	CA	-50,2001	-18,3752	-31,8248
130	GLU	HA	130	GLU	CA	-22,6551	-17,2101	-5,445
132	GLN	HA	132	GLN	CA	15,0858	9,5217	5,5641
133	SER	HA	133	SER	CA	52,6144	20,2934	32,321
134	ALA	HA	134	ALA	CA	39,2655	19,4693	19,7962
135	LEU	HA	135	LEU	CA	38,2522	16,7745	21,4777
136	SER	HA	136	SER	CA	29,2045	10,0038	19,2007
137	ASP	HA	137	ASP	CA	-3,7417	-20,0775	16,3358
139	GLU	HA	139	GLU	CA	23,9118	5,1717	18,7401
140	THR	HA	140	THR	CA	-29,4593	-2,4392	-27,0201
142	LYS	HA	142	LYS	CA	-11,963	-16,1031	4,1401
143	ASN	HA	143	ASN	CA	14,3272	-1,2455	15,5727
144	TYR	HA	144	TYR	CA	27,6884	7,9562	19,7322
146	SER	HA	146	SER	CA	32,8802	8,2228	24,6574
147	ASP	HA	147	ASP	CA	-23,1542	-22,8414	-0,3128
148	ALA	HA	148	ALA	CA	41,5222	24,3746	17,1477
149	PHE	HA	149	PHE	CA	22,2041	22,7873	-0,5832
151	PHE	HA	151	PHE	CA	-21,7522	-2,4131	-19,3391
154	GLU	HA	154	GLU	CA	10,1893	16,8017	-6,6125
155	GLN	HA	155	GLN	CA	32,2509	16,518	15,7329
157	LEU	HA	157	LEU	CA	2,4039	22,1398	-19,7359
158	GLN	HA	158	GLN	CA	-21,6862	-10,3667	-11,3194
159	LEU	HA	159	LEU	CA	-7,642	-8,2267	0,5847
161	GLU	HA	161	GLU	CA	46,3848	15,662	30,7228
162	THR	HA	162	THR	CA	45,347	15,5711	29,7759
163	THR	HA	163	THR	CA	-0,9199	3,4008	-4,3207
164	ALA	HA	164	ALA	CA	-14,1923	2,7517	-16,944
166	PRO	HA	166	PRO	CA	31,8528	23,7345	8,1183
167	GLU	HA	167	GLU	CA	-7,624	-2,6347	-4,9893
169	GLU	HA	169	GLU	CA	33,2019	-3,8264	37,0284
170	ALA	HA	170	ALA	CA	3,0521	12,2815	-9,2295
172	ASN	HA	172	ASN	CA	-2,2039	1,834	-4,0379
173	LEU	HA	173	LEU	CA	-0,1915	5,4141	-5,6057
176	ILE	HA	176	ILE	CA	52,7559	24,5907	28,1652

177	THR	HA	177	THR	CA	-6,4409	-11,5471	5,1062
178	GLN	HA	178	GLN	CA	-18,553	-7,3974	-11,1556
179	ASN	HA	179	ASN	CA	-41,4222	0,0869	-41,5091
180	ARG	HA	180	ARG	CA	-32,2792	-5,5216	-26,7576
181	GLN	HA	181	GLN	CA	-16,3811	-12,0528	-4,3283
182	ALA	HA	182	ALA	CA	6,1136	-4,0372	10,1508
183	LEU	HA	183	LEU	CA	18,4077	7,8347	10,573
185	ASP	HA	185	ASP	CA	-20,7616	-19,9733	-0,7883
186	ILE	HA	186	ILE	CA	20,5418	20,809	-0,2673
188	ALA	HA	188	ALA	CA	1,8105	9,4935	-7,683
189	ILE	HA	189	ILE	CA	11,7224	0,8688	10,8536
192	ASP	HA	192	ASP	CA	31,1612	6,9414	24,2199
194	ASN	HA	194	ASN	CA	-16,4491	-12,56	-3,8891
195	LYS	HA	195	LYS	CA	-7,9882	-7,6631	-0,3251
196	VAL	HA	196	VAL	CA	-17,2633	-5,56	-11,7033
198	MET	HA	198	MET	CA	-43,7016	-14,5732	-29,1283
200	SER	HA	200	SER	CA	-23,0466	-10,0893	-12,9574
203	GLN	HA	203	GLN	CA	-16,4142	-16,2849	-0,1293
205	SER	HA	205	SER	CA	-31,9632	-9,6656	-22,2976
207	THR	HA	207	THR	CA	28,3941	-1,0393	29,4334
208	GLN	HA	208	GLN	CA	23,8146	1,4966	22,318
209	PRO	HA	209	PRO	CA	-19,8474	19,293	-39,1404
210	LEU	HA	210	LEU	CA	-7,1023	-4,3452	-2,7571
211	TYR	HA	211	TYR	CA	-2,1171	1,6177	-3,7348
212	THR	HA	212	THR	CA	0,2113	-1,5793	1,7907
213	LEU	HA	213	LEU	CA	2,3124	-3,9622	6,2745
214	ASP	HA	214	ASP	CA	-25,0118	-1,8593	-23,1526
216	ASP	HA	216	ASP	CA	25,7977	-6,7459	32,5437
218	THR	HA	218	THR	CA	-7,5853	15,7309	-23,3163
219	LEU	HA	219	LEU	CA	-2,4869	-2,9605	0,4736
220	THR	HA	220	THR	CA	-6,5494	-3,0979	-3,4515
221	ASN	HA	221	ASN	CA	-13,1961	2,3476	-15,5437
222	ASN	HA	222	ASN	CA	6,6947	14,5918	-7,897
224	SER	HA	224	SER	CA	18,5558	-8,2613	26,8171
226	VAL	HA	226	VAL	CA	-16,2349	-4,1813	-12,0536
227	LYS	HA	227	LYS	CA	-10,9072	-12,7703	1,8631
232	ASN	HA	232	ASN	CA	-7,2806	-7,6332	0,3526
234	ILE	HA	234	ILE	CA	-41,008	8,0285	-49,0365
236	PHE	HA	236	PHE	CA	-13,4942	-11,1054	-2,3888
237	TYR	HA	237	TYR	CA	6,8712	-0,259	7,1301
238	GLN	HA	238	GLN	CA	32,6887	13,4121	19,2766
239	SER	HA	239	SER	CA	-5,7135	-6,649	0,9355
240	ILE	HA	240	ILE	CA	-20,7003	-8,623	-12,0772
241	THR	HA	241	THR	CA	7,2655	-6,6419	13,9074
245	ASN	HA	245	ASN	CA	13,9518	15,3704	-1,4187
246	TRP	HA	246	TRP	CA	-18,5086	-13,854	-4,6546
248	ASP	HA	248	ASP	CA	-11,9158	-9,9523	-1,9635
249	GLU	HA	249	GLU	CA	18,1435	21,7843	-3,6408
250	LYS	HA	250	LYS	CA	22,2466	16,447	5,7996
251	LEU	HA	251	LEU	CA	31,3301	-4,5468	35,877
252	SER	HA	252	SER	CA	-20,2634	-17,0324	-3,231
255	TYR	HA	255	TYR	CA	-15,2915	-4,3163	-10,9752
256	THR	HA	256	THR	CA	9,7553	7,4145	2,3408
257	VAL	HA	257	VAL	CA	-10,8733	5,5547	-16,428
261	TRP	HA	261	TRP	CA	1,0435	6,8695	-5,826
262	LYS	HA	262	LYS	CA	0,2962	-5,6421	5,9383

264	PHE	HA	264	PHE	CA	4,2701	13,4218	-9,1517
267	VAL	HA	267	VAL	CA	-1,385	-8,1744	6,7894
268	PHE	HA	268	PHE	CA	6,9042	24,2663	-17,3622
269	THR	HA	269	THR	CA	7,6344	-22,6378	30,2722
271	GLU	HA	271	GLU	CA	0,1557	0,1144	0,0413
273	ILE	HA	273	ILE	CA	0,7576	-8,1909	8,9485
274	GLN	HA	274	GLN	CA	0,3038	-0,9022	1,206

HaCa domain 1 (in absence of MalE)

ID_I	RES_I	ATOM_I	ID_J	RES_J	ATOM_J	D_OBS	D	D_DIFF
99	GLN	HA	99	GLN	CA	-0,55	-16,9029	16,3529
100	LEU	HA	100	LEU	CA	-1,0142	-5,5261	4,5119
101	THR	HA	101	THR	CA	-33,8123	-18,6824	-15,1299
102	PHE	HA	102	PHE	CA	31,6103	30,528	1,0823
103	GLU	HA	103	GLU	CA	-24,5175	-15,3146	-9,2029
104	ARG	HA	104	ARG	CA	-8,5401	-13,2118	4,6716
105	ALA	HA	105	ALA	CA	20,0587	12,8743	7,1844
106	GLN	HA	106	GLN	CA	14,0036	10,0725	3,9312
107	GLU	HA	107	GLU	CA	-12,8432	-8,5236	-4,3196
108	VAL	HA	108	VAL	CA	-28,3592	-16,3177	-12,0415
112	ARG	HA	112	ARG	CA	-28,8951	-4,052	-24,8431
113	SER	HA	113	SER	CA	3,5228	10,3102	-6,7874
209	PRO	HA	209	PRO	CA	-19,8474	-14,6673	-5,18
210	LEU	HA	210	LEU	CA	-7,1023	2,5982	-9,7005
211	TYR	HA	211	TYR	CA	-2,1171	-5,657	3,5399
212	THR	HA	212	THR	CA	0,2113	-6,44	6,6514
213	LEU	HA	213	LEU	CA	2,3124	4,0255	-1,7131
214	ASP	HA	214	ASP	CA	-25,0118	-18,3338	-6,678
216	ASP	HA	216	ASP	CA	25,7977	22,9441	2,8537
218	THR	HA	218	THR	CA	-7,5853	-12,0126	4,4272
219	LEU	HA	219	LEU	CA	-2,4869	-3,0688	0,5819
220	THR	HA	220	THR	CA	-6,5494	-2,6887	-3,8607
221	ASN	HA	221	ASN	CA	-13,1961	-10,6589	-2,5372
222	ASN	HA	222	ASN	CA	6,6947	-3,3972	10,0919
224	SER	HA	224	SER	CA	18,5558	15,4528	3,103
226	VAL	HA	226	VAL	CA	-16,2349	-14,0553	-2,1796
227	LYS	HA	227	LYS	CA	-10,9072	-10,6437	-0,2636
232	ASN	HA	232	ASN	CA	-7,2806	-10,9678	3,6872
234	ILE	HA	234	ILE	CA	-41,008	-17,6768	-23,3313
236	PHE	HA	236	PHE	CA	-13,4942	-14,975	1,4809
237	TYR	HA	237	TYR	CA	6,8712	20,9522	-14,0811
238	GLN	HA	238	GLN	CA	32,6887	23,4358	9,2529
239	SER	HA	239	SER	CA	-5,7135	-10,4281	4,7145
240	ILE	HA	240	ILE	CA	-20,7003	-16,6952	-4,005
241	THR	HA	241	THR	CA	7,2655	-17,2999	24,5654
245	ASN	HA	245	ASN	CA	13,9518	-2,4771	16,4289
246	TRP	HA	246	TRP	CA	-18,5086	-12,7173	-5,7914
248	ASP	HA	248	ASP	CA	-11,9158	-7,7523	-4,1635
249	GLU	HA	249	GLU	CA	18,1435	12,4163	5,7272
250	LYS	HA	250	LYS	CA	22,2466	21,2936	0,9529
251	LEU	HA	251	LEU	CA	31,3301	29,4644	1,8657
252	SER	HA	252	SER	CA	-20,2634	-8,1504	-12,113
255	TYR	HA	255	TYR	CA	-15,2915	-14,0981	-1,1934
256	THR	HA	256	THR	CA	9,7553	11,1278	-1,3725
257	VAL	HA	257	VAL	CA	-10,8733	24,4621	-35,3354

HaCa domain 2 (in absence of MalE)

ID_I	RES_I	ATOM_I	ID_J	RES_J	ATOM_J	D_OBS	D	D_DIFF
118	LYS	HA	118	LYS	CA	-3,6559	13,5424	-17,1983
119	THR	HA	119	THR	CA	-42,7336	-25,519	-17,2146
120	TYR	HA	120	TYR	CA	-48,7038	-22,1961	-26,5076
121	ASN	HA	121	ASN	CA	10,9497	10,3201	0,6296
127	ALA	HA	127	ALA	CA	-50,2001	-29,0521	-21,148
130	GLU	HA	130	GLU	CA	-22,6551	-26,4454	3,7904
132	GLN	HA	132	GLN	CA	15,0858	20,1916	-5,1058
133	SER	HA	133	SER	CA	52,6144	42,3982	10,2162
134	ALA	HA	134	ALA	CA	39,2655	41,2252	-1,9597
135	LEU	HA	135	LEU	CA	38,2522	36,9575	1,2948
136	SER	HA	136	SER	CA	29,2045	26,3082	2,8963
137	ASP	HA	137	ASP	CA	-3,7417	-26,0826	22,3409
139	GLU	HA	139	GLU	CA	23,9118	-6,3148	30,2266
140	THR	HA	140	THR	CA	-29,4593	-17,0154	-12,4438
142	LYS	HA	142	LYS	CA	-11,963	-14,6987	2,7357
143	ASN	HA	143	ASN	CA	14,3272	8,9374	5,3899
144	TYR	HA	144	TYR	CA	27,6884	22,978	4,7104
146	SER	HA	146	SER	CA	32,8802	23,7203	9,1599
147	ASP	HA	147	ASP	CA	-23,1542	-30,5254	7,3712
148	ALA	HA	148	ALA	CA	41,5222	37,5605	3,9617
149	PHE	HA	149	PHE	CA	22,2041	29,581	-7,3769
151	PHE	HA	151	PHE	CA	-21,7522	-11,0636	-10,6886
154	GLU	HA	154	GLU	CA	10,1893	12,3992	-2,2099
155	GLN	HA	155	GLN	CA	32,2509	27,0851	5,1658
157	LEU	HA	157	LEU	CA	2,4039	28,6593	-26,2554
158	GLN	HA	158	GLN	CA	-21,6862	-11,8436	-9,8425
159	LEU	HA	159	LEU	CA	-7,642	-7,0984	-0,5436
161	GLU	HA	161	GLU	CA	46,3848	34,5117	11,873
162	THR	HA	162	THR	CA	45,347	31,7932	13,5538
163	THR	HA	163	THR	CA	-0,9199	5,0613	-5,9811
164	ALA	HA	164	ALA	CA	-14,1923	-10,8301	-3,3622
166	PRO	HA	166	PRO	CA	31,8528	43,6133	-11,7605
167	GLU	HA	167	GLU	CA	-7,624	-11,5653	3,9412
169	GLU	HA	169	GLU	CA	33,2019	-24,352	57,5539
170	ALA	HA	170	ALA	CA	3,0521	25,0288	-21,9767
172	ASN	HA	172	ASN	CA	-2,2039	-18,8717	16,6678
173	LEU	HA	173	LEU	CA	-0,1915	18,912	-19,1035
176	ILE	HA	176	ILE	CA	52,7559	37,9488	14,8071
177	THR	HA	177	THR	CA	-6,4409	-9,6693	3,2283
178	GLN	HA	178	GLN	CA	-18,553	-4,848	-13,7049
179	ASN	HA	179	ASN	CA	-41,4222	-22,5336	-18,8886
180	ARG	HA	180	ARG	CA	-32,2792	-16,3116	-15,9676
181	GLN	HA	181	GLN	CA	-16,3811	-11,3062	-5,0749
182	ALA	HA	182	ALA	CA	6,1136	-6,216	12,3296
183	LEU	HA	183	LEU	CA	18,4077	22,9559	-4,5482
185	ASP	HA	185	ASP	CA	-20,7616	-18,8074	-1,9542
186	ILE	HA	186	ILE	CA	20,5418	26,9167	-6,375
188	ALA	HA	188	ALA	CA	1,8105	9,8521	-8,0416
189	ILE	HA	189	ILE	CA	11,7224	1,76	9,9624
192	ASP	HA	192	ASP	CA	31,1612	19,5715	11,5897
194	ASN	HA	194	ASN	CA	-16,4491	-13,8866	-2,5625
195	LYS	HA	195	LYS	CA	-7,9882	-7,0192	-0,969

196	VAL	HA	196	VAL	CA	-17,2633	-4,1208	-13,1425
198	MET	HA	198	MET	CA	-43,7016	-32,5798	-11,1218
200	SER	HA	200	SER	CA	-23,0466	-12,5828	-10,4639
203	GLN	HA	203	GLN	CA	-16,4142	-17,2617	0,8475
205	SER	HA	205	SER	CA	-31,9632	-15,5202	-16,443
207	THR	HA	207	THR	CA	28,3941	-11,2603	39,6544

HnN all (in presence of MalE)

ID_I	RES_I	ATOM_I	ID_J	RES_J	ATOM_J	D_OBS	D	D_DIFF
101	THR	H	101	THR	N	14,4257	7,851	6,5747
102	PHE	H	102	PHE	N	9,0571	5,2349	3,8222
103	GLU	H	103	GLU	N	2,6068	-1,1174	3,7241
107	GLU	H	107	GLU	N	3,0227	1,4052	1,6174
113	SER	H	113	SER	N	-10,6368	-7,128	-3,5088
116	ALA	H	116	ALA	N	-4,3288	-2,6765	-1,6523
117	GLY	H	117	GLY	N	-2,22	-7,9192	5,6992
123	GLY	H	123	GLY	N	-7,6853	-7,6975	0,0122
125	TYR	H	125	TYR	N	-15,3122	-0,0116	-15,3006
127	ALA	H	127	ALA	N	3,5298	7,0628	-3,533
130	GLU	H	130	GLU	N	10,7317	8,4383	2,2934
132	GLN	H	132	GLN	N	4,192	-7,1603	11,3523
134	ALA	H	134	ALA	N	-16,0565	-5,3283	-10,7282
135	LEU	H	135	LEU	N	-3,8126	-1,3052	-2,5073
136	SER	H	136	SER	N	-4,4528	-1,9891	-2,4638
137	ASP	H	137	ASP	N	1,5724	1,3459	0,2266
138	GLY	H	138	GLY	N	7,3332	6,9599	0,3733
140	THR	H	140	THR	N	-1,1438	-2,3253	1,1815
141	GLY	H	141	GLY	N	11,5216	6,8781	4,6435
146	SER	H	146	SER	N	-4,462	-7,9908	3,5288
147	ASP	H	147	ASP	N	14,2195	7,6353	6,5842
148	ALA	H	148	ALA	N	-10,604	4,0423	-14,6463
152	GLY	H	152	GLY	N	-5,022	-3,1704	-1,8516
159	LEU	H	159	LEU	N	5,79	10,2699	-4,48
161	GLU	H	161	GLU	N	-12,4318	-6,1854	-6,2465
164	ALA	H	164	ALA	N	1,9592	-1,9874	3,9466
168	GLY	H	168	GLY	N	9,5131	8,0134	1,4997
170	ARG	H	170	ARG	N	-0,6202	-1,7731	1,1529
171	ALA	H	171	ALA	N	-7,5485	-2,3446	-5,2038
177	THR	H	177	THR	N	29,4898	6,9302	22,5596
182	ALA	H	182	ALA	N	-2,3532	0,2282	-2,5814
188	ALA	H	188	ALA	N	4,7739	-5,793	10,5669
190	LEU	H	190	LEU	N	12,2914	12,3197	-0,0283
193	GLY	H	193	GLY	N	21,4415	-5,0886	26,5301
196	VAL	H	196	VAL	N	9,6463	0,6712	8,9751
198	MET	H	198	MET	N	-4,2704	-5,5195	1,249
200	SER	H	200	SER	N	10,3213	2,0012	8,32
203	GLN	H	203	GLN	N	9,6773	2,3779	7,2994
204	PHE	H	204	PHE	N	-3,8162	4,1405	-7,9567
205	SER	H	205	SER	N	1,4812	-4,0427	5,5239
206	GLY	H	206	GLY	N	3,8089	-5,1563	8,9652
210	LEU	H	210	LEU	N	-12,1673	-8,4733	-3,6941
211	TYR	H	211	TYR	N	-1,5214	-0,3614	-1,16
213	LEU	H	213	LEU	N	10,0604	3,8084	6,252
214	ASP	H	214	ASP	N	0,7406	0,6305	0,1101
215	GLY	H	215	GLY	N	1,2003	-2,9884	4,1887
217	GLY	H	217	GLY	N	15,1608	6,8867	8,2741
219	LEU	H	219	LEU	N	9,9893	3,9744	6,0148
220	THR	H	220	THR	N	4,8724	5,4117	-0,5392
221	ASN	H	221	ASN	N	16,0145	9,2361	6,7784
222	ASN	H	222	ASN	N	-9,6992	-7,4073	-2,2919
225	GLY	H	225	GLY	N	1,6436	-0,9722	2,6158

226	VAL	H	226	VAL	N	-1,3864	3,8978	-5,2841
228	TYR	H	228	TYR	N	10,9725	2,5062	8,4663
234	ILE	H	234	ILE	N	4,1099	-0,0902	4,2001
238	GLN	H	238	GLN	N	-9,3636	-1,3327	-8,0308
240	ILE	H	240	ILE	N	18,313	13,34	4,973
241	THR	H	241	THR	N	14,2816	10,433	3,8485
245	ASN	H	245	ASN	N	-4,2339	-5,1605	0,9266
247	GLY	H	247	GLY	N	2,1489	-7,293	9,4419
248	ASP	H	248	ASP	N	-3,2069	-3,3631	0,1562
250	LYS	H	250	LYS	N	1,2459	-5,0949	6,3409
254	GLY	H	254	GLY	N	-6,6783	0,3609	-7,0392
256	THR	H	256	THR	N	13,5355	8,6437	4,8917
260	GLY	H	260	GLY	N	-5,6477	4,7252	-10,3729
262	LYS	H	262	LYS	N	-0,5546	-2,5616	2,0071
264	PHE	H	264	PHE	N	-7,782	-6,7192	-1,0628
268	PHE	H	268	PHE	N	-3,0227	-3,7211	0,6984
272	GLY	H	272	GLY	N	3,2306	-3,9453	7,1759
273	ILE	H	273	ILE	N	-1,0671	-7,0461	5,9789
274	GLN	H	274	GLN	N	-2,8184	-8,4047	5,5864
275	LYS	H	275	LYS	N	-4,2029	2,0697	-6,2726

HnN domain 1 (in presence of MalE)

ID_I	RES_I	ATOM_I	ID_J	RES_J	ATOM_J	D_OBS	D	D_DIFF
101	THR	H	101	THR	N	14,4257	10,3552	4,0705
102	PHE	H	102	PHE	N	9,0571	6,6535	2,4036
103	GLU	H	103	GLU	N	2,6068	1,7926	0,8142
107	GLU	H	107	GLU	N	3,0227	4,592	-1,5694
113	SER	H	113	SER	N	-10,6368	-13,6775	3,0407
210	LEU	H	210	LEU	N	-12,1673	-10,3925	-1,7748
211	TYR	H	211	TYR	N	-1,5214	0,927	-2,4484
213	LEU	H	213	LEU	N	10,0604	6,1865	3,8739
214	ASP	H	214	ASP	N	0,7406	5,1175	-4,3769
215	GLY	H	215	GLY	N	1,2003	-1,7811	2,9814
217	GLY	H	217	GLY	N	15,1608	10,7476	4,4133
219	LEU	H	219	LEU	N	9,9893	7,4082	2,5811
220	THR	H	220	THR	N	4,8724	9,8767	-5,0043
221	ASN	H	221	ASN	N	16,0145	13,5799	2,4346
222	ASN	H	222	ASN	N	-9,6992	-11,2325	1,5333
225	GLY	H	225	GLY	N	1,6436	0,1866	1,457
226	VAL	H	226	VAL	N	-1,3864	-3,0499	1,6636
228	TYR	H	228	TYR	N	10,9725	7,0365	3,936
234	ILE	H	234	ILE	N	4,1099	1,1107	2,9992
238	GLN	H	238	GLN	N	-9,3636	-2,9797	-6,3839
240	ILE	H	240	ILE	N	18,313	17,7546	0,5584
241	THR	H	241	THR	N	14,2816	14,3771	-0,0955
245	ASN	H	245	ASN	N	-4,2339	-6,5582	2,3243
247	GLY	H	247	GLY	N	2,1489	-4,2467	6,3956
248	ASP	H	248	ASP	N	-3,2069	-1,0343	-2,1726
250	LYS	H	250	LYS	N	1,2459	-7,1241	8,37
254	GLY	H	254	GLY	N	-6,6783	1,8947	-8,5731
256	THR	H	256	THR	N	13,5355	13,0739	0,4616

HnN domain 2 (in presence of MalE)

ID_I	RES_I	ATOM_I	ID_J	RES_J	ATOM_J	D_OBS	D	D_DIFF
117	GLY	H	117	GLY	N	-2,22	-10,5358	8,3158
123	GLY	H	123	GLY	N	-7,6853	-5,5277	-2,1576
125	TYR	H	125	TYR	N	15,3122	3,7715	-19,0838
127	ALA	H	127	ALA	N	3,5298	7,8324	-4,3026
130	GLU	H	130	GLU	N	10,7317	6,7928	3,9389
132	GLN	H	132	GLN	N	4,192	-3,8048	7,9968
134	ALA	H	134	ALA	N	16,0565	-6,0873	-9,9692
135	LEU	H	135	LEU	N	-3,8126	-2,3885	-1,4241
136	SER	H	136	SER	N	-4,4528	-3,7367	-0,7161
137	ASP	H	137	ASP	N	1,5724	0,6421	0,9304
138	GLY	H	138	GLY	N	7,3332	7,5005	-0,1673
140	THR	H	140	THR	N	-1,1438	-3,6406	2,4968
141	GLY	H	141	GLY	N	11,5216	4,7306	6,791
146	SER	H	146	SER	N	-4,462	-6,7683	2,3063
147	ASP	H	147	ASP	N	14,2195	8,3234	5,8961
148	ALA	H	148	ALA	N	10,604	2,3651	-12,9691
152	GLY	H	152	GLY	N	-5,022	-2,4382	-2,5837
159	LEU	H	159	LEU	N	5,79	7,4122	-1,6222
161	GLU	H	161	GLU	N	12,4318	-4,2393	-8,1925
164	ALA	H	164	ALA	N	1,9592	3,4119	-1,4527
168	GLY	H	168	GLY	N	9,5131	9,8277	-0,3145
170	ARG	H	170	ARG	N	-0,6202	0,3523	-0,9725
171	ALA	H	171	ALA	N	-7,5485	-1,6842	-5,8643
177	THR	H	177	THR	N	29,4898	8,9569	20,5329
182	ALA	H	182	ALA	N	-2,3532	-0,6201	-1,7331
188	ALA	H	188	ALA	N	4,7739	-3,4443	8,2182
190	LEU	H	190	LEU	N	12,2914	9,4203	2,8711
193	GLY	H	193	GLY	N	21,4415	-2,4792	23,9207
196	VAL	H	196	VAL	N	9,6463	-0,0477	9,694
198	MET	H	198	MET	N	-4,2704	-2,8528	-1,4176
200	SER	H	200	SER	N	10,3213	0,3161	10,0052
203	GLN	H	203	GLN	N	9,6773	0,5894	9,0879
204	PHE	H	204	PHE	N	-3,8162	3,8992	-7,7154
205	SER	H	205	SER	N	1,4812	-3,8609	5,3421
206	GLY	H	206	GLY	N	3,8089	-3,2759	7,0848